

Multi-model assessment of the deglacial climatic evolution at high southern latitudes

Takashi Obase^{1,2}, Laurie Menviel³, Ayako Abe-Ouchi¹, Tristan Vadsaria¹⁴, Ruza Ivanovic⁵, Brooke Snoll⁵, Sam Sherriff-Tadano⁵, Paul J. Valdes⁶, Lauren Gregoire⁵, Marie-Luise Kapsch⁷, Uwe Mikolajewicz⁷, Nathaëlle Bouttes⁸, Didier Roche⁸, Fanny Lhardy⁸, Chengfei He⁹, Bette Otto-Bliesner¹⁰, Zhengyu Liu¹¹, Wing-Le Chan¹

¹Atmosphere and Ocean Research Institute, The University of Tokyo, Kashiwa, Japan

²Japan Agency for Marine-Earth Science and Technology, Yokohama, Japan

³Climate Change Research Center, The Australian Centre for Excellence in Antarctic Science, the University of New South Wales, Sydney, Australia,

⁴UiT The Arctic University of Norway, Tromsø, Norway

⁵School of Earth & Environment, University of Leeds, Woodhouse Lane, Leeds, UK

⁶School of Geographical Sciences, University of Bristol, University Road, Bristol, UK

⁷Max Planck Institute for Meteorology, Hamburg, Germany

⁸Laboratoire des Sciences du Climat et de l'Environnement/Institut Pierre-Simon Laplace, UMR CEA-CNRS-UVSQ, Université Paris-Saclay, Gif-sur-Yvette, France

⁹Woods Hole Oceanographic Institution, Woods Hole, MA, USA

¹⁰Climate and Global Dynamics Laboratory, National Center for Atmospheric Research, Boulder, USA

¹¹Atmospheric Science Program, Department of Geography, Ohio State University, Columbus, USA

Correspondence to: Takashi Obase (tobase@jamstec.go.jp)

Abstract. The quaternary climate is characterised by glacial-interglacial cycles, with the most recent transition from the last glacial maximum to the present interglacial (the last deglaciation) occurring between ~ 21 and 9 ka. While the deglacial warming at high southern latitudes is mostly in phase with atmospheric CO₂ concentrations, some proxy records have suggested that the onset of the warming occurred before the CO₂ increase. In addition, high southern latitudes exhibit a cooling event in the middle of the deglaciation (15 - 13 ka) known as the “Antarctic Cold Reversal” (ACR). In this study, we analyse transient simulations of the last deglaciation performed by six different climate models as part of the 4th phase of the Paleoclimate Modelling Intercomparison Project (PMIP4) to understand the processes driving high southern latitude surface temperature changes. As the protocol of the last deglaciation sets the choice of freshwater forcing as flexible, the freshwater forcing is different in each model, thus hindering the multi-model comparison. While proxy records from West Antarctica and the Pacific sector of the Southern Ocean suggest the presence of an early warming before 18 ka, only half the models show

a significant warming ($\sim 1^{\circ}\text{C}$ or $\sim 10\%$ of the total deglacial warming). All models simulate a major warming during Heinrich stadial 1 (HS1, 18 - 15 ka) concurrent with the CO_2 increase and with an AMOC weakening in some models. However, the simulated HS1 warming over Antarctica is smaller than the one suggested from ice core data. During the ACR, simulations with an abrupt AMOC increase exhibit a high southern latitude cooling of 1 to 2°C , in relative agreement with proxy records, while simulations with rapid North Atlantic meltwater input exhibit a warming. Using simple models to extract the relative AMOC contribution, we find that all climate models simulate a high southern latitude cooling in response to an AMOC increase with a response timescale of several hundred years, suggesting the choice of the North Atlantic meltwater forcing substantially affects high southern latitudes temperature changes. Thus, further work needs to be carried out to reconcile the deglacial AMOC evolution with the Northern hemisphere ice sheet disintegration and associated meltwater input. Finally, all simulations exhibit only minimal changes in Southern Hemisphere westerlies and Southern Ocean meridional circulation during the last deglaciation. Improved understanding of the processes impacting southern high atmospheric and oceanic circulation changes accounting for deglacial atmospheric CO_2 increase are needed.

1. Introduction

The recent Quaternary climate is characterised by glacial-interglacial cycles of about 100,000-year periodicity (Lisiecki and Raymo, 2005; Jouzel et al., 2007). These glacial-interglacial cycles are driven by insolation changes as external forcing and by feedbacks, including changes in atmospheric greenhouse gas (GHG) concentrations and continental ice sheets (Abe-Ouchi et al., 2013). During the Last Glacial Maximum (LGM, ~ 21 ka; ka indicates 1000 years before present), the continental ice sheets covered a significant area of the high northern latitudes (Tarasov et al., 2012; Peltier et al., 2015), thus leading to a sea level fall of ~ 130 meters compared to pre-industrial (Lambeck et al., 2014). The atmospheric CO_2 concentration was also ~ 100 ppm lower than pre-industrial (Petit et al., 1999; Bereiter et al., 2015). These climatic boundary conditions contributed to a colder climate during the LGM, with global mean surface air temperature anomalies estimated to be 4 to 7°C lower than present-day (Annan et al., 2022; Liu et al., 2023). As the last deglaciation (transition from the LGM to the early Holocene) represents one of the largest, most recent and well-documented natural warming of the last million years,

an understanding of the processes and feedbacks during this time period can offer insight into our own modern changing world. Here, we focus on the high southern latitudes, where deglacial warming began before their Northern Hemisphere (NH) counterparts (Shakun et al., 2012), and which have been suggested to play a major role in driving the increase in atmospheric CO₂ concentration. Although the timing of the onset of the deglacial warming at high southern latitudes is poorly constrained, a compilation of Antarctic ice core records from East Antarctica suggests that the deglacial Antarctic warming started at ~ 18 ka, in phase with the rise in atmospheric CO₂ concentration (Parrenin et al., 2013). On the other hand, a record from the West Antarctic Ice Sheet Divide ice core (WDC) suggests that the warming started at ~ 20 ka (Shakun et al., 2012; WAIS project members, 2013). Moreover, an early onset of the deglacial warming (~21 ka) at high and mid-southern latitudes has also been suggested based on SST and sea ice records from the Pacific sector of the Southern Ocean (Moy et al., 2019; Sikes et al., 2019; Moros et al., 2021; Crosta et al., 2022; Sadatzki et al., 2023).

Millennial-scale climate events are superimposed on the deglacial warming. At the beginning of the deglaciation, during Heinrich stadial 1 (HS1, ~18 to 14.7 ka, following Ivanovic et al., 2016), Greenland and the North Atlantic region remained cold (Buizert et al., 2014; Martrat et al., 2007), while significant warming occurred at high southern latitudes (WAIS project members, 2010). This period was associated with a weakening of the Atlantic Meridional Ocean Circulation (AMOC), evidenced by Pa/Th in marine sediments (McManus et al., 2004; Ng et al., 2018). During the subsequent Bølling-Allerød (BA, ~14.7 to 12.8 ka) period, Greenland surface air temperatures rose by more than 10°C in just a few decades (Stephensen et al., 2008; Buizert et al., 2014), and the AMOC strengthened significantly (Severinghaus & Brook, 1999; McManus et al., 2004; Roberts et al., 2010; Ng et al., 2018). A cooling event at high southern latitudes, known as the Antarctic Cold Reversal (ACR), was identified between ~15 and 13 ka (Jouzel et al. 2007; Pedro et al., 2016), concurrent with the BA. The Younger-Dryas (YD, 12.8 to 11.7 ka) followed the BA, and was characterised by a drastic cooling in Greenland and the North Atlantic. While the processes leading to the YD are still debated (Renssen et al., 2015), it has been suggested that the YD could be attributed to a weakening of the AMOC (McManus et al., 2004), caused by a rerouting of freshwater into the Arctic that was then transported toward the deep-water formation sites of the subpolar North Atlantic by coastal boundary currents (Condrón and Winsor, 2012; Kapsch et al., 2022).

88 Climate model simulations with marine proxy constraints support the variations in the AMOC during the
89 last deglaciation (Pöppelmeier et al., 2023).

90 An AMOC weakening causes a warming in the South Atlantic as the meridional oceanic heat
91 transport to the North Atlantic is weakened (Stocker & Johnsen, 2003; Stouffer et al., 2006). This
92 warming can then be propagated to the Southern Ocean and Antarctica (Pedro et al., 2018). The
93 contrasting temperature changes between Greenland and the southern high latitudes can also be found
94 during abrupt events of the last glacial period known as Dansgaard–Oeschger cycles (Dansgaard 1993;
95 NGRIP project members, 2004; WAIS Divide project members, 2015), which have led to the notion of a
96 bipolar seesaw (Stocker and Johnsen 2003; Capron et al., 2010). Alongside these events, the atmospheric
97 CO₂ increase throughout the deglaciation occurred in steps, suggesting a link to millennial-scale climate
98 events (Marcott et al., 2014) and changes in Southern Ocean circulation contributing to degassing of
99 oceanic carbon (Anderson et al., 2009, Menviel et al., 2018).

100 Transient climate simulations provide a suitable framework for assessing the processes leading to
101 deglacial climate changes. Early transient simulations that were conducted with transient orbital forcing,
102 GHGs and ice sheets suggested that an increase in austral spring insolation in the southern high latitudes
103 was responsible for the onset of warming (Timmermann et al., 2009), and that deglacial warming of the
104 Southern Ocean appeared as early as ~20 to 18 ka in association with sea ice retreat (Roche et al., 2011).
105 Transient simulations that also included freshwater input into the North Atlantic highlighted the AMOC
106 impact on climate change (Liu et al., 2009; He et al., 2011). Menviel et al. (2011) further showed that the
107 ACR could be a response to the strong AMOC increase at the end of HS1, but that its length and amplitude
108 could have been enhanced by meltwater input from the Antarctic ice sheet. These simulations were
109 designed to simulate AMOC changes in agreement with estimates from proxy records, and therefore the
110 magnitude, location, and timing of the implemented meltwater fluxes were idealised. In contrast,
111 experiments forced with meltwater fluxes consistent with ice sheet reconstructions based on sea-level
112 constraints often simulate millennial-scale AMOC changes in disagreement with accepted interpretations
113 of climate and ocean records (Snoll et al., 2024). Some experiments simulate an AMOC weakening at the
114 time of the BA because of significant mass loss of NH ice sheets (Bethke et al., 2012; Ivanovic et al.,
115 2018a; Kapsch et al., 2022; Bouttes et al., 2023) or do not simulate any abrupt climate events (Gregoire

et al., 2012). With an idealised scenario that follows the evolution of NH ice sheets more closely (except for the 14 ka meltwater pulse), the MIROC climate model shows that it is possible to simulate an abrupt AMOC strengthening with the presence of continuous freshwater in the North Atlantic because of gradual warming (Obase and Abe-Ouchi, 2019). These studies indicate that different models have different sensitivities in terms of the AMOC response to forcing and, therefore, it is useful to analyse multi-model results for a robust understanding of the climatic processes.

To facilitate further examination of the mechanisms driving deglacial climate change, a protocol for carrying out transient simulations of the last deglaciation was proposed as part of the fourth phase of the Paleoclimate Modeling Intercomparison Project (PMIP4) (Ivanovic et al., 2016). The protocol of PMIP4 deglaciation summarised climate forcings needed (ice core based atmospheric GHGs and reconstructed ice sheets) for climate model experiments. The protocol is designed to be flexible in that the use of some boundary conditions is determined by each modelling group, which allows an exploration of different climate scenarios. The first PMIP multi-model study of the last deglaciation, focusing on the northern hemispheric climate during HS1, found that different freshwater approaches (*melt-uniform*, *melt-routed*, *trace-like*, *bespoke*, Snoll et al. (2024)) have a dominant impact on North Atlantic climate variability. While this finding could be drawn due to the flexibility of the PMIP deglaciation protocol (Ivanovic et al., 2016) regarding the choice of the method on how to distribute the freshwater forcing, this flexibility makes it challenging to properly compare the simulations. Nevertheless, the multi-model assessment of the last deglaciation performed here provides an opportunity to investigate the processes impacting southern high latitude climate and to evaluate the uncertainties from the models' sensitivity to the forcings.

Some boundary conditions for climate models, including GHG and Antarctic ice sheet (prescribed in PMIP4 protocol), result from climate change at high southern latitudes. Proxy records (Sigman et al., 2010, Skinner et al., 2010, Martinez-Garcia et al., 2011) and modelling studies (Bouttes et al., 2012, Menviel et al., 2016, Menviel et al., 2018, Gottschalk et al., 2019) indicate that physical and biogeochemical changes in the Southern Ocean may have significantly contributed to ocean carbon uptake during the last glacial period and to the atmospheric CO₂ increase during HS1. Subsurface warming on the Antarctic shelf contributes to the mass loss of Antarctic ice sheets through enhanced melting of ice

shelves, and retreat of grounding lines (Golledge et al., 2014; Lowry et al., 2019). In addition, climate conditions at high southern latitudes can impact the formation of Antarctic Bottom Water (AABW) and the shoaling of AMOC (Sherriff-Tadano et al., 2023). Hence investigating the deglacial climate evolution at high southern latitudes may give an insight into critical climate system feedback.

Here, we analyse the deglacial climatic evolution (21–11 ka) at high southern latitudes as simulated in six PMIP4 transient experiments, and compare the results with paleo-proxy records. We focus on the magnitude and rate of Antarctic surface air temperature (SAT) and Southern Ocean sea surface temperature (SST) changes. As there is a substantial difference between the AMOCs in the simulations, we utilise statistical or simple models to separate the impact of changes in atmospheric CO₂ and AMOC on Southern Ocean SST. Finally, we analyse the evolution of the AABW, Southern Ocean westerlies and subsurface ocean temperature in the Southern Ocean to discuss critical climate system feedbacks occurring at high southern latitudes.

2 Methods

2-1 Climate models and experiments used in this study

We use the PMIP4 transient simulations of the last deglaciation performed with six atmosphere-ocean coupled climate models (Table 1). Table 2 summarises the experimental design of each model simulation and their reference articles, with the evaluation of their LGM and PI states mentioned in their description. These simulations are initialised with glacial conditions, and the LGM climate fields have been evaluated by previous studies, particularly for global temperature changes (Kageyama et al. 2021), sea ice and SST changes in the Southern Ocean (Lhardy et al., 2021; Green et al. 2022), and SAT changes over the Antarctic ice sheet (Buizert et al. 2021). A part of the transient simulations utilized in this study have also been compared to proxy-reconstructions (Weitzel et al. 2024). Fig. S1 compares simulated sea-ice edges for the pre-industrial simulations from six models used in this study, which shows models simulate reasonable sea ice extents. The Equilibrium Climate Sensitivity (ECS, defined by global mean SAT changes in response to doubling CO₂ from the pre-industrial) of each model ranges from 2.0 to 3.9 °C, and the global mean surface air temperature (SAT) anomaly for the LGM is 3.5 to 7.3 °C (Table 1). While some of the modelling groups performed two or more sensitivity experiments with different

model parameters or boundary conditions (e.g., different freshwater forcing (FWF) scenarios or ice sheets), for this study we have selected one representative simulation from each climate model. Fig. 1 summarises the time evolution of the climate forcings, i.e. insolation, atmospheric GHGs, and continental ice sheets used in the simulations. Both reconstructions (ICE-6G_C VM5a, henceforth ‘ICE-6G_C’; and ‘GLAC-1D’) have larger Antarctic ice sheet volume at the LGM, with a ~ 10 m sea-level equivalent volume change at the LGM, relative to present-day. Both suggest ~ 100 m of elevation change since the LGM at EPICA Dome C (EDC, 123°E, 75°S), while WAIS Divide (WDC, 112°W, 79.5°S) differs by 300 m between the two datasets (Fig. 1d).

Fig. 2a summarises the total amount of FWF in the NH in six simulations. The FWF schemes can be classified into two groups: [a] FWF adjusted to reproduce large-scale AMOC variability (iTRACE, LOVECLIM, MIROC) and [b] FWF consistent with the reconstructed ice volume changes (HadCM3, MPI-ESM, iLOVECLIM) based on ICE-6G_C or GLAC-1D (Fig. 2a, black lines). Notably, during HS1, iTRACE and LOVECLIM have significant FWF (~ 0.2 Sv), while other simulations apply FWF of less than 0.1 Sv. In LOVECLIM and MIROC, the meltwater flux was uniformly applied to the North Atlantic, while other models use the location of the melting NH ice-sheet and associated runoff to apply a spatially varying FWF (Table 2). ICE-6G_C (HadCM3, MPI-ESM, iLOVECLIM) leads to a meltwater input of about 0.1 Sv to the Southern Ocean at 11.5–11 ka. iTRACE and LOVECLIM also applied freshwater flux to the Southern Ocean to simulate the ACR (iTRACE: up to 0.2Sv during 14.4–13.9 ka, LOVECLIM: fixed at 0.09Sv during 14.67–14.1 ka).

In section 3.3, we conduct further analysis to examine the processes driving Southern Ocean SST using a multilinear regression (MLR) model and a thermal bipolar seesaw model adapted from Stocker and Johnsen (2003).

2-2: Simple models to disentangle CO₂ and AMOC

2-2-1: Multilinear Regression model

We use a MLR model to regress changes in SST onto CO₂ and AMOC variations:

$$SST = \alpha_I * CO_2 + \beta_I * AMOC + \gamma, (1)$$

where *SST*, and *AMOC* (defined as the maximum meridional overturning streamfunction in the North Atlantic, at depths below 500 m and 20–60°N) are output from the climate models, and *CO*₂ is the forcing used in each simulation. γ is the intercept. The AMOC in the analysis is normalised with respect to the maximum and minimum values in each model. The *CO*₂ is also normalised with respect to the total change between 21 and 11 ka (~83 ppm). The MLR analysis is applied to the 2-D fields of the Southern Ocean SST. The same analysis is applied to the Southern Ocean SST averaged over 55–40°S. Every 100-years, mean SST, AMOC, and *CO*₂ from 20 to 11 ka are used as the input for this analysis, so each dataset has 90 time-slices. While we use *CO*₂ as a representation of a gradual forcing as the input of the MLR model, we note that other forcing, such as from ice sheets and orbital changes can contribute to the warming. On the other hand, sensitivity experiments evaluating the contribution of each forcing show that they have a minor impact on Southern Ocean SST and Antarctic SAT changes between 19 and 15 ka (He et al. 2013).

2-2-2: Thermal bipolar seesaw model

As the MLR model does not consider transient climate response, we construct a thermal bipolar seesaw model following Stocker and Johnsen (2003). The original thermal bipolar seesaw model is based on an energy balance between the North and South Atlantic Oceans. We add the effect of *CO*₂ on temperature, which was not considered in the original model. The thermal bipolar seesaw model in this study solves the temporal evolution of Southern Ocean SST using the following equations:

$$\frac{d\Delta SST}{dt} = \frac{\Delta SST_{eq} - \Delta SST(t)}{\tau} \quad (2)$$

$$\Delta SST_{eq} = \alpha_2 * CO_2(t) + \beta_2 * m(t) \quad (3)$$

where ΔSST_{eq} is an equilibrium Southern Ocean SST (change since the LGM) expected from the *CO*₂ and state of the AMOC at time *t*. $\Delta SST(t)$ is the SST change since LGM at time *t*, and τ is the characteristic timescale of the bipolar seesaw. *CO*₂(*t*) is the *CO*₂ concentration at time *t*, and is normalised with maximum and minimum values as in the MLR model. The term *m*(*t*) represents the modes of the AMOC from the climate model outputs. When using the simulated AMOC within the bipolar seesaw model, it is assumed that the AMOC has only two modes, unlike the continuous values in the model. Based on Figure 2, we assume that the AMOC is in a strong mode (*m*(*t*)=0) if the AMOC is greater than 14 Sv.

At first, we conduct systematic sensitivity experiments to calculate the minimum root mean square error between the actual ΔSST and the bipolar seesaw models. We conduct 9610 sensitivity experiments

for each model within the parameter ranges shown in Table 3. The combination of parameters that gives the minimum root mean square error, along with coefficient of determination between the climate models' SST changes and bipolar seesaw models are displayed in Table 5.

3. Results

3-1: AMOC

As AMOC variations can impact southern high latitude climate, we summarise here the transient evolution of the AMOC in the different simulations. As detailed below, the AMOC evolution is substantially affected by the FWF schemes. All simulations except for MIROC display a strong (~ 20 Sv) AMOC at the LGM (Fig. 2b), while MPI-ESM and iLOVECLIM shows slightly weaker LGM AMOC if GLAC-1D ice sheet was used (Kapsch et al., 2022; Bouttes et al., 2023). The more vigorous LGM AMOC compared to Pre-Industrial (PI) is in line with the majority of PMIP4 simulations (Kageyama et al., 2021), although it is not consistent with LGM reconstructions from multiple marine tracers (Lynch-Stieglitz et al., 2007; Bohm et al., 2015; Menviel et al., 2016). During the period corresponding to HS1, the AMOC stays weak in MIROC and significantly declines in the iTRACE and LOVECLIM simulations, as meltwater is added into the North Atlantic. On the other hand, in the other simulations, there is only a slight reduction in AMOC (~ 1 Sv) as the meltwater input into the North Atlantic stays below 0.05 Sv. At the BA (~ 14.7 ka), three models exhibit an abrupt change from weak to strong AMOC, triggered by a rapid reduction in FWF (iTRACE and LOVECLIM) or as a response to the gradual background warming (MIROC). These simulations, featuring an AMOC strengthening, broadly agree with marine proxy records (Fig. 2b black line). On the other hand, the other three simulations (HadCM3, MPI-ESM, iLOVECLIM) display an AMOC weakening due to a significant increase in FWF originating from the ice sheet collapse associated with Meltwater Pulse 1a (Deschamps et al., 2012). During the Younger-Dryas (12.8–11.7 ka), iTRACE, LOVECLIM, and MIROC simulate an AMOC decline, corresponding to an increase in FWF or an oscillatory nature of the AMOC in MIROC (Kuniyoshi et al., 2022). HadCM3 simulates a gradual AMOC reduction, while MPI-ESM exhibits multi-centennial AMOC variability. At 11 ka, the AMOC strength returns to a strong mode except for iLOVECLIM, which stays weak after the BA.

256 **3-2-1: 21–18 ka (onset of warming) and 18–14.7 ka (HS1)**

257 Fig. 3 summarises the simulated Antarctic SAT and Southern Ocean SST changes since the LGM
 258 in all the simulations (LGM is defined as 21 ka in most models, with some exceptions because of different
 259 initialisation; 20.6 ka for LOVECLIM, 20.0 ka for iTRACE). The SAT at WDC and EDC are compared
 260 with the ice core based reconstructions from Parrenin et al. (2013) and Buizert et al., (2021). Three models
 261 (MIROC, HadCM3, MPI-ESM) exhibit a gradual $\sim 1^\circ\text{C}$ warming between 21 and 18 ka at both WDC and
 262 EDC (Fig. 3c). This simulated EDC warming is comparable with EDC ice core estimates (Parrenin et al.,
 263 2013). However, the magnitude of warming suggested from WDC ($\sim 2^\circ\text{C}$ warming between 19.5–19 ka,
 264 Shakun et al., 2012) is not simulated by any of the models, with iTRACE exhibiting slight cooling (Fig.
 265 4a). MIROC, HadCM3 and MPI-ESM also simulate a significant SAT increase over Antarctica and a
 266 $0.5\text{--}1.0^\circ\text{C}$ SST increase in the Southern Ocean north of the sea ice edge, with a gradual reduction in
 267 Southern Ocean sea ice area (Figs. 3f and 4).

268 All models exhibit a larger warming between 18 and 14.7 ka (i.e. HS1) than between 21 and 18
 269 ka. iTRACE simulates the largest warming ($+6\text{--}8^\circ\text{C}$), closely following the estimates from ice core data.
 270 The sharp increase in temperature in iTRACE starts at ~ 18 ka, corresponding to a period of major
 271 reduction in AMOC strength (Fig. 3b). The warming in MPI-ESM follows iTRACE with a 5°C warming,
 272 despite a minor reduction in AMOC strength. The HadCM3 exhibits $\sim 4^\circ\text{C}$ warming at WDC and $\sim 2^\circ\text{C}$
 273 warming at EDC, while the other models simulate a $2\text{--}4^\circ\text{C}$ warming at EDC and WDC (Fig. 3c–d).
 274 iTRACE exhibits the most significant Southern Ocean SST increase of 5°C and LOVECLIM exhibits a
 275 sharp Southern Ocean SST increase of $\sim 3^\circ\text{C}$, in response to an AMOC reduction at ~ 17 ka. The other
 276 models' Southern Ocean SST increase by $1\text{--}2^\circ\text{C}$ (Fig. 3e). Southern Ocean sea ice area exhibits the same
 277 trends as the Southern Ocean SST, with iTRACE simulating the largest sea ice area reduction of up to
 278 40% compared to the LGM (Figs 3f and 4b).

279 **3-2-2: 14.7–13 ka (BA) and 13–11 ka (YD and Holocene onset)**

280 Three models (iTRACE, MIROC, LOVECLIM) simulate an abrupt AMOC increase at the BA
 281 onset, and a concomitant cooling at high southern latitudes: $\sim 1\text{--}2^\circ\text{C}$ Antarctic SAT and Southern Ocean
 282 SST decrease. iTRACE and LOVECLIM exhibit a sharp cooling in Southern Ocean SST and SAT in the

early phase of the BA, probably enhanced by the meltwater flux into the Southern Ocean (Menviel et al., 2011). In contrast, the three other models (HadCM3, MPI-ESM, iLOVECLIM) exhibit a warming in the early phase of the BA, corresponding to an AMOC weakening. Subsequently, HadCM3 and MPI-ESM exhibit a gradual cooling over the Antarctic and Southern Ocean as the AMOC strengthens in the later part of the BA (~13.5 ka). iLOVECLIM displays a rapid warming at 13.5 ka, followed by a cooling, which is explained by abrupt surface albedo changes caused by the evolving land-sea mask in the Antarctic region (Bouttes et al., 2023).

During YD (13–11ka), iTRACE, MIROC, and LOVECLIM simulate an AMOC weakening as well as a high southern latitude warming. iTRACE simulates a ~3–4°C increase in Southern Ocean SST, while LOVECLIM and MIROC simulate a 1°C warming. MPI-ESM exhibits multi-centennial variability associated with variations in AMOC strength. MPI-ESM and iLOVECLIM exhibit sharp cooling in Southern Ocean SST and SAT starting at ~11.5 ka, enhanced by the meltwater flux into the Southern Ocean (Kapsch et al., 2022).

The total deglacial (21–11 ka) warming is 10 °C in WDC, while the EDC estimates range from 5 to 10 °C (Parrenin et al., 2013; Buizert et al., 2021). Across the simulations, a 2 to 10 °C warming is simulated over Antarctica. In line with the WDC and the upper range of EDC estimates, iTRACE and MPI-ESM display a 8–10 °C total warming over Antarctica. The Southern Ocean sea ice edge retreats poleward by 10° latitude in most models. A SST increase of up to 6 °C is simulated in this area in iTRACE, LOVECLIM, HadCM3, and MPI-ESM, while a ~4 °C SST increase is simulated in MIROC and iLOVECLIM (Fig. 5).

The different magnitudes of warming during HS1 and YD between models could be explained by the range of temperature changes between LGM and PI, as the mean SAT and SST changes are different by a factor of two (Table 1). To reduce this model difference, Antarctic SAT are normalised by the temperature anomaly between LGM and PI in Figure 6. When normalised, the simulations with a weak AMOC during HS1 show the largest warming over Antarctica (Fig. 6 left). The normalised Antarctic SAT change at 11 ka lies in between 0.6 and 0.8 with respect to the total temperature change between LGM and PI for five out of six models. This indicates that warming occurred after the onset of the Holocene, which marks a difference between the simulations and proxy data, in that the temperature at

11 ka is comparable to the pre-industrial values based on ice core reconstructions (Parrenin et al., 2013; Buizert et al., 2021).

3-3: SST – CO₂ – AMOC relationship analysis

The simulated AMOC time series display large differences across simulations due to different FWF schemes, which complicates the quantification of CO₂ forcing and AMOC changes in driving high southern latitude temperature changes in each model. To overcome this, we examine the Southern Ocean SST trajectory against CO₂ forcing, and AMOC strength (Fig. 7). Fig. 7 shows that the deglacial increase in atmospheric CO₂ has significant impacts on the Southern Ocean SST because the temperature trajectory is mostly proportional to CO₂ changes unless there are significant AMOC changes. Temperature changes associated with changes in AMOC are superimposed on Southern Ocean SSTs, in that an AMOC weakening (blue circles) tends to induce a warming, and vice versa. Even though the actual time series of AMOC in each model are very different, this result suggests that high southern latitude temperature changes can be decomposed into the effects of CO₂ and AMOC. The relative importance of CO₂ and AMOC are quantified in the following subsections.

3-4: Results of MLR model

The results of the MLR model indicate that the CO₂ coefficients range from 1.0 to 6.5°C for the total deglacial CO₂ changes (Table 4). All models have a negative coefficient of AMOC (–0.3 to –2.4°C), indicating a Southern Ocean SST increase associated with an AMOC weakening. The negative coefficient of AMOC in all models suggest that an AMOC shutdown during HS1 has the potential to explain about half of the SST changes.

The regression against Southern Ocean 2-D SST fields indicates that the CO₂ coefficient is mostly positive over the Southern Ocean, ranging from ~0.5 °C in the Antarctic zone where sea ice is present until 11 ka, to 2–6 °C in the Southern Ocean north of the LGM winter sea ice edge (Fig. 8). The sensitivity to the AMOC is mostly negative in the Southern Ocean, and areas of high sensitivity overlap with those of CO₂, suggesting sea ice modulates the areas sensitive to both CO₂ and AMOC changes.

3-5: Results of bipolar seesaw model

Table 5 summarises the results of the bipolar seesaw model. All models have positive CO₂ coefficients (2.0–6.0°C) and negative AMOC coefficients (–0.5 to –2.9°C), as in the MLR models. The time series simulated by the bipolar seesaw model are compared with actual SST changes and with MLR models in Fig. 9. The bipolar seesaw model succeeds in reproducing a gradual SST decrease as a result of an AMOC strengthening (e.g. gradual cooling in iTRACE and MIROC, 15–13 ka). This gradual cooling was not represented by the MLR model, which exhibits an immediate SST response to AMOC changes. The response time ranges from 100–700 years, with most models ranging from 500–700 years with the exception of LOVECLIM and iLOVECLIM (Table 5).

We note that the values of the CO₂ sensitivity from the MLR and bipolar seesaw model may include gradual forcing from other greenhouse gases, ice sheets, and orbital forcing. In addition, a sharp cooling associated with freshwater in the Antarctic Ocean was not represented because both models, MLR and bipolar seesaw, do not consider meltwater in the Southern hemisphere (~14.5 ka of iTRACE and LOVECLIM, ~11.5 ka of MPI-ESM and iLOVECLIM)

3-6: Other Southern Ocean climate variables

We analyse AABW transport (minimum global meridional overturning streamfunction, at depths below 3000 m and 60°S–30°S) as an indicator of Southern Ocean meridional circulation, and 850 hPa zonal mean winds over the Southern Ocean (zonal mean winds averaged over 65°S–40°S). We focus on the onset of deglaciation (21–18 ka) and the initial significant increase in CO₂ (~HS1, 18–15 ka). The AABW (Fig. 10b) at the LGM ranges from 10 to 30 Sv among the six models and stays relatively constant between 21 and 18 ka. In the subsequent period (18–15 ka), iTRACE exhibits a significant decline in the AABW, in phase with Southern Ocean SST changes (Fig. 10d). LOVECLIM and MPI-ESM exhibit a gradual decline in AABW (~5 Sv), while three other models (MIROC, HadCM3, iLOVECLIM) exhibit a small reduction or a stable AABW. The zonal winds over the Southern Ocean do not change significantly between 21 and 18 ka, apart from MIROC and MPI-ESM, which exhibit a slight weakening (Fig. 10c). Between 18 and 15 ka, the zonal winds continue to decline in MIROC and MPI-ESM, and start to decline in iTRACE and LOVECLIM. Little changes in zonal winds are simulated in iLOVECLIM, while HadCM3 exhibits a ~10% strengthening.

Subsurface ocean temperatures south of 60°S at depths of around 500 m (Fig. 10e) exhibit an increase during HS1 in 4 of the 6 simulations, with the largest warming (1.2 °C and 0.8 °C) simulated by the two simulations which exhibited the largest SST increase (iTRACE and MPI-ESM). During the ACR (15–13 ka), iTRACE and MIROC exhibit a gradual sub-surface temperature decrease while HadCM3 and MPI-ESM exhibit a continuous warming, as per the SST changes in the respective models. iLOVECLIM and LOVECLIM exhibit small changes (<0.5°C) in the total sub-surface temperature. Abrupt subsurface warming in iTRACE (~14 ka) and LOVECLIM (14.8–14.2 ka) coincide with Southern Ocean SST reduction, suggesting that this results from enhanced Southern Ocean stratification as a response to Southern Ocean meltwater input (Menviel et al., 2011; Lowry et al., 2018).

3-7: Additional freshwater experiments on HS1 SO warming in MIROC and HadCM3

We additionally show two simulations run with the MIROC and HadCM3 models to assess the impact on southern high latitude climate of a significant AMOC decrease during HS1. In the MIROC simulations, the FWF during HS1 is increased to 0.1 Sv or 0.2 Sv between 18 and 15.5 ka (Figure 11a, red and orange lines) instead of 0.03 Sv in the standard simulation. This larger meltwater input further weakens the AMOC (Figure 11a) and leads to an additional 1 °C SST increase in the SO compared to the standard simulation. The 1 °C warming in response to AMOC reduction of ~5 Sv is significantly higher than results from the MLR and bipolar seesaw models. In the HadCM3 simulations, a North Atlantic freshwater flux of ~0.2 Sv during HS1 (similar to Trace-21ka A, Liu et al., 2009) significantly reduces the AMOC (Figure 11b blue lines), and induces an additional ~1 °C increase in Southern Ocean SST compared to the standard simulation. The results from the MIROC and HadCM3 sensitivity experiments show that the simulated warming during HS1 can be twice as strong with an AMOC shutdown compared to the standard simulation of each model. As in the LOVECLIM Heinrich stadial 4 simulation (Figure S2; Margari et al. 2020) the warming in the southern high latitude in response to AMOC strength is not necessarily linear, while MLR models assume a linear temperature response to the AMOC.

4. Discussion

4-1: Onset of deglacial warming

The climate forcing in the early deglaciation primarily comes from insolation due to obliquity and precession changes (Fig. 1a), which leads to an increase in spring to summer insolation south of 60 °S (Fig. S2). Ice core data suggest that the onset of deglacial warming at WDC was earlier than the increase in CO₂, and this early deglacial warming has been suggested to result from an AMOC reduction (Shakun et al., 2012) or local insolation changes (WAIS project members, 2013). However, simulated early warming is smaller than proxy records. Three models (MIROC, HadCM3, MPI-ESM) exhibit a small but significant warming (~ 0.5°C) between 21 and 18 ka (Fig. 4a) in both West and East Antarctica, as well as at the surface of the Southern Ocean, primarily in the Pacific sector (Fig. 4b) as suggested by proxy records (Moy et al., 2019; Sikes et al., 2019; Moros et al., 2021). The amplitude of the early warming in these models is comparable to a previous modelling study (Timmermann et al., 2009), while the other models show a slight cooling (iTRACE) or little change (LOVECLIM and iLOVECLIM).

The first explanation for the differences in the simulated temperature change between 21 and 18 ka is the Southern Ocean sea ice at LGM. MIROC, HadCM3 and MPI-ESM have less LGM summer sea ice than other models. The smaller sea ice extent at the LGM, relative to other models, may lead to a high sensitivity to increased insolation during austral spring to summer, causing significant warming with sea ice retreat (Timmermann et al., 2009; Roche et al., 2011). If the LGM Southern Ocean sea ice extent is extensive, the increase in insolation primarily south of 60 °S (Fig. S2) does not warm the Southern Ocean as much because of high sea ice albedo. Although the local insolation changes are the likely cause of an early warming simulated in some of the models, the addition of freshwater could contribute to the AMOC weakening. For example, the consideration of an additional freshwater flux from the Fennoscandian ice sheet in the freshwater forcing prior to 18ka as included in MPI and as suggested by Touccane et al. (2010), would weaken the AMOC and lead to a more pronounced warming in the southern high latitudes.

Another model-data difference is the different early warming rates between West and East Antarctica. The data from WDC suggest there was significant warming in West Antarctica, while a less significant change in East Antarctica is suggested by EDC. In contrast, the models simulate similar warming rates in both West and East Antarctica (Fig. 4a), suggesting the models may underestimate the spatial heterogeneity in West and East Antarctic warming. This might be attributed to the Antarctic ice sheet history prescribed in the experiments, where both ICE-6G_C and GLAC-1D have minor surface

elevation changes at WDC in the early deglaciation (Fig. 1d). Buizert et al. (2021) used the MIROC and HadCM3 models and showed that the uncertainty in Antarctic ice sheet height affects the difference between LGM and PI temperatures because changes in surface elevation affect SAT (~1 °C per 100 m). This might suggest that the lower surface elevations at WDC, related to the ice sheet terminus retreat between 20–15 ka in the Amundsen Sea (Bentley et al. 2014), may have contributed to the early deglacial warming primarily in West Antarctica. The coarse resolution of the atmospheric models (2.5 to 5.6 degrees in the horizontal) may impact the warming contrast between EAIS and WAIS through an inherent smoothing of the surface topography of the Antarctic ice sheet and the associated impact on the atmospheric circulation. In addition, the relatively coarse resolution of the ocean models (1 to 3 degrees), may impact the AMOC sensitivity to iceberg and freshwater flux in the North Atlantic (Condrón and Winsor 2012), or parameterizations of mesoscale processes in the Southern Ocean and their response to the deglaciation.

Uncertainty in the Antarctic ice sheet topography could also explain some model-data differences during the early Holocene, where simulations indicate that an additional warming occurs after the onset of the Holocene (Fig. 6). This is different from ice core data (Fig. 4) and global mean ocean temperature (including deep-sea temperature) estimated from noble gases in ice cores, which suggests that temperatures reach Holocene levels at the end of YD (Bereiter et al., 2018). The higher surface elevation of the Antarctic ice sheet at 11 ka compared to the present-day in the experimental design (Fig. 1e) may contribute to the simulated Holocene warming. It would be valuable to assess the uncertainties from ice sheet reconstructions, as new reconstructions have been published (e.g., Gowan et al., 2021), and different LGM ice sheets can induce different AMOC variabilities (Prange et al., 2023; Masoum et al., 2024).

4-2: Rate of temperature changes

HS1 (~18–14.7 ka) exhibits significant warming in all models because of the CO₂ increase, with the total warming being dependent on the sensitivity of each model to CO₂ and to AMOC changes. iTRACE simulates the largest warming during HS1 among six models, with an Antarctic SAT increase of 6–8°C and Southern Ocean SST of 4–5°C. While the Antarctic SAT matches ice-core data, Southern Ocean SST is larger than the SST stack. Five models besides iTRACE simulates a Southern Ocean SST change which compare well with the SST stack data, but these five models underestimate Antarctic SAT.

448 This indicates that the different magnitudes of warming between Southern Ocean SST and Antarctic SAT
449 are weakly simulated in models. While iTRACE exhibits the largest global mean SAT changes at the
450 LGM (7.3 °C, compared to the six-model mean of 5.3 °C), the ECS of iTRACE (3.6 °C) is not the highest
451 among the six models; instead, MIROC4m has the highest ECS despite weaker deglacial warming (Table
452 1). We examine the relationship between ECS and the LGM global mean SAT changes using multi-model
453 PMIP3 and PMIP4 simulations (Fig. S3). We find a weak negative correlation (-0.06) between the ECS
454 and global mean LGM SAT changes, and the local SAT change in the individual climate models can vary
455 by about a factor of two even with the same ECS. A substantial asymmetry between warm and cold
456 climates has been identified in previous studies because of the presence of continental ice sheets, ocean
457 dynamics, and cloud feedback (Yoshimori et al., 2009; Zhu and Poulsen, 2021). Hence, understanding
458 the mechanism and amplitude of cooling in the LGM simulations will contribute to a better understanding
459 of multi-model differences in the deglacial warming.

460 The sensitivity to AMOC ranges between (-0.5 to -2.9°C) based on the analysis using the thermal
461 bipolar seesaw model (Table 5). A multi-model study comparing freshwater hosing experiments of 11
462 climate models (including LOVECLIM, MIROC, and HadCM3 used in this study) under LGM climate
463 shows that most models exhibit warming in the Southern Ocean (Kageyama et al., 2013). However, the
464 simulation length in their study is less than 420 years, as opposed to the estimated timescale in this study
465 (~ 500 – 700 years), suggesting the need for longer simulations to evaluate the extent of the climate
466 response at high southern latitudes.

467 The MLR and thermal bipolar seesaw models in this study include several assumptions. Firstly,
468 as the gradual forcing is represented only by the CO_2 concentration, they do not consider the effect from
469 retreating ice sheets, meltwater flux in the Southern Ocean, or insolation changes explicitly. Other
470 forcings besides CO_2 and AMOC, could be included in the CO_2 or AMOC coefficients, for instance, other
471 gradual forcings have positive correlations with the CO_2 forcing. Antarctic and Northern Hemisphere ice
472 sheet changes could impact Southern Ocean SST through deep-water formation. This may explain the
473 CO_2 coefficients from the MLR and bipolar seesaw model that are higher than expected from ECS value.
474 On the other hand, the AMOC sensitivity of the LOVECLIM model is low compared to the 1.5°C

Southern Ocean SST increase found in the simulation of Heinrich stadial 4 (Margari et al. 2020, Fig. S4), and the CO₂ coefficient is quite high, potentially implying a poor separations of the two factors.

As shown here, the deglacial AMOC variations are quite different amongst the simulations. Only those which display an AMOC increase at the end of HS1 can capture a cooling trend corresponding to the ACR as suggested by ice-core data (iTRACE, LOVECLIM, MIROC). In comparison to previous transient simulations of the last deglaciation, the representation of the duration of the ACR has improved, as it was previously simulated as too short (Lowry et al., 2018). On the other hand, simulations that are forced with a large NH meltwater pulse consistent with ice sheet reconstructions do not simulate an ACR (Ivanovic et al., 2016; 2018; Kapsch et al., 2022; Bouttes et al., 2023). This so-called meltwater paradox (Ivanovic et al., 2018; Snoll et al., 2024) suggests a need for a better assessment of freshwater scenarios, and the potential sensitivity of climate models to freshwater forcing. We also note that the routing location of meltwater input (Roche et al., 2010; He et al., 2020) and the consideration of icebergs and meltwater discharge into the ocean (Schloesser et al., 2019; Love et al., 2021) may induce quite different AMOC changes. Southern FWF can enhance the ACR, as found in iTRACE (~14.2 ka) and LOVECLIM (~14.7 ka), with a sharp cooling in Southern Ocean SST and Antarctic SAT primarily in WDC. This is caused by the intensified stratification in the Southern Ocean (Menviel et al., 2010; 2011), which induces significant warming in the subsurface and contributes to further mass loss from Antarctic ice sheets (Golledge et al., 2014). As ice core data does not exhibit such sharp cooling events as compared to climate model simulations (Fig. 3), this may provide some constraints on the extent and duration of FWF from the Antarctic ice sheet.

4-3: Implications for climate system changes at high southern latitudes

Reconstructions have suggested that changes in Southern Ocean circulation, probably driven by wind changes, were important for the modulation of Southern Ocean CO₂ outgassing during the deglaciation. Proxies suggest an enhanced opal flux during HS1, which could reflect increased upwelling in the Southern Ocean due to changes in Southern Hemispheric westerlies (SHW) (Anderson et al., 2009), and poleward shift of the SHW across the deglaciation (Gray et al., 2023). Proxies also suggest decreasing deep and intermediate-depth Southern Ocean ventilation ages (Skinner et al., 2010, Burke et al., 2011),

503 increasing intermediate-depth pH in the Southern Ocean during HS1 (Rae et al., 2018). It has been
504 suggested that stronger or poleward-shifted SHW and/or enhanced AABW formation during HS1 would
505 indeed enhance Southern Ocean CO₂ outgassing and lead to an atmospheric CO₂ increase (Menviel et al.,
506 2014; Menviel et al., 2018). In contrast, in the present study, most models show very little change or a
507 gradual weakening in the SHW across the deglaciation, and there is little latitudinal migration of the SHW.
508 Only the HadCM3 model displays a SHW strengthening during HS1. However, additional studies should
509 look in more details into potential changes in the location of the SHW in these simulations, as well as
510 regional changes in SHW strength and their relation to other climatic variables (Rojas et al., 2009; Sime
511 et al., 2013). In addition, no model exhibits an increase in AABW, which could contribute to the upwelling
512 of carbon-rich water mass in the deep ocean and CO₂ outgassing from the Southern Ocean. Instead, the
513 deglaciation may have contributed to the long-term weakening in AABW by warming the Southern Ocean,
514 enhancing sea ice melt, and decreasing surface salinity (Marson et al., 2016). While it has been suggested
515 that larger Southern Ocean sea ice extent would lead to an atmospheric CO₂ decrease at the LGM
516 (Marzocchi et al., 2020, Stein et al., 2020), few models simulate significant changes in oceanic CO₂ due
517 to a Southern Ocean sea ice change (Gottschalk et al., 2019). These physical changes still need to be
518 reconciled with processes put forward to explain the deglacial atmospheric CO₂ changes by running
519 coupled climate-carbon simulations.

520 Finally, we also find that changes in subsurface ocean temperature in the Southern Ocean, one of
521 the critical factors impacting the retreat of the Antarctic ice sheet, display significant differences across
522 the simulations. This could be related to different ECS or FWF in the Southern Ocean, and should also
523 be investigated in future studies to quantify uncertainties in subsurface ocean temperature changes.
524 Model-dependent subsurface ocean temperature change is one source of uncertainty in projecting future
525 Antarctic ice sheet mass loss (Serrousi et al., 2020). In contrast to the present simulations of the last
526 deglaciation, which prescribe the Antarctic ice sheet history, climate variability occurring during the
527 deglaciation can impact the Antarctic ice sheet, which can act as feedback to Southern Ocean climate via
528 meltwater input from the Antarctic ice sheet (Menviel et al., 2010; Golledge et al., 2014; Clark et al.,
529 2020). Hence, further coupled climate and ice sheet modelling studies are needed to improve our

understanding of climatological and glaciological processes and to evaluate model performance under a warming climate and rising sea levels (Gomez et al., 2020).

5. Conclusion

In our multi-model analysis of transient deglacial experiments, the early increase in Antarctic SAT is weakly simulated or absent. The multi-model difference could be related to the smaller LGM sea ice extent, which may affect the sensitivity to insolation change, or to a slight reduction in the AMOC in response to small freshwater input from NH ice sheets. In addition, the different warming rates between West and East Antarctica suggested by ice core records are not reproduced by the transient simulations. In all models, a major warming occurs between 18 and 15 ka in response to increased CO₂ concentration. The multi-model analysis and sensitivity experiments further suggest that the AMOC reduction during HS1 associated with increased freshwater flux in the North Atlantic contributes to a larger warming, in agreement with high southern latitude proxy records, even though no simulation can reproduce both the amplitude of Southern Ocean SST and Antarctic SAT changes simultaneously. The bipolar seesaw model indicates all models have bipolar seesaw response, and an abrupt AMOC increase at the end of HS1 is necessary to simulate the high southern latitude cooling corresponding to the ACR. The simulations do not exhibit significant changes in winds over the Southern Ocean or meridional circulation in the Southern Ocean, which could contribute to enhanced CO₂ outgassing from the Southern Ocean. This indicates the necessity for future climate system modelling studies to quantify the sequence of deglacial climate changes and atmospheric CO₂ increase.

Acknowledgements:

We thank the two anonymous referees for their valuable comments which have substantially improved our paper. TO, AAO, TV and WLC acknowledge funding from JSPS Kakenhi 17H06104, 17H06323, and JPJSBP120213203. TO was also supported by JPMXD0722680395 and JSPS kakenhi 24H00026. We acknowledge discussions at PAGES-QUIGS T5–T0 workshops, supported by INQUA Terminations Five to Zero (T5–T0) Working Group (Project #2004). LM acknowledges funding from Australian Research Council (ARC) grants FT180100606 and SR200100008. UM and MK acknowledge funding by the German Federal Ministry of Education and Research as a Research for Sustainability

Initiative through the PalMod project (grant nos. 01LP1915C, and 01LP1917B). The MLR analysis used scikit-learn library of Python 3.7. The figures were created using Generic Mapping Tool (GMT version 4 and 6).

Data availability:

All model data supporting our findings will be archived at Zenodo. Original model data is upon request for authors from each modelling group.

Code availability:

The bipolar seesaw model and the MLR model used in this study can be shared upon request.

Author contribution:

TO, LM, and AAO conceived the study. TO, LM, TV, BS analysed the data. TO, LM, AAO, TV, RI, and BS wrote the manuscript with input from all co-authors.

Competing interests:

Laurie Menviel is a member of the editorial board of Climate of the Past, but otherwise all authors declare that they have no conflict of interest.

References:

Name	Climate model name	ECS [K]	Global mean	
			LGM SAT anomaly [K]	References
iTRACE	iCESM1.3	3.6	7.3	Tierney et al., (2020)
LOVECLIM	LOVECLIM	2.8	4.2	McDougall et al., (2020), Goosse et al., (2010)
MIROC	MIROC4m	3.9	4.5	Chan and Abe-Ouchi, (2020)
HadCM3	HadCM3B	2.7	6.1	Kageyama et al., (2021)
MPI-ESM	MPI-ESM-CR P2		6.1	
iLOVECLIM	iLOVECLIM	2.0	3.5	

Table 1: Summary of climate models analysed in this study. Note that the ECS for MPI-ESM (model version MPI-ESM-CR P2) has not been calculated.

Name	Freshwater scheme	GHGs	Ice sheets	References for deglaciation experiments
iTRACE	TraCE-like	PMIP4	ICE-6G_C	He et al., 2019; 2021
LOVECLIM	TraCE-like	Kohler et al., 2017	ICE-5G	Menviel et al., 2011
MIROC	ICE-6G_C with adjustment	PMIP4	ICE-5G (LGM fix)	Obase and Abe-Ouchi 2019; Obase et al., 2021
HadCM3	ICE-6G_C	PMIP4	Ice-6G_C	Ivanovic et al., 2018; Snoll et al., 2022
MPI-ESM	ICE-6G_C	Kohler et al., 2017	Ice-6G_c	Kapsch et al., 2022
iLOVECLIM	ICE-6G_C	PMIP4	Ice-6G_c	Bouttes et al., 2023

577 **Table 2:** Summary of the experimental design used in the transient deglacial simulations.

Parameter [unit]	Range
CO ₂ coefficient α [K/83 ppm]	1.0–7.0, every 0.2
AMOC coefficient β [K/(normalised AMOC)]	0.0–3.0, every 0.1
Response timescale τ [year]	100–1000, every 100

579 **Table 3:** Parameter ranges in the thermal bipolar seesaw model.

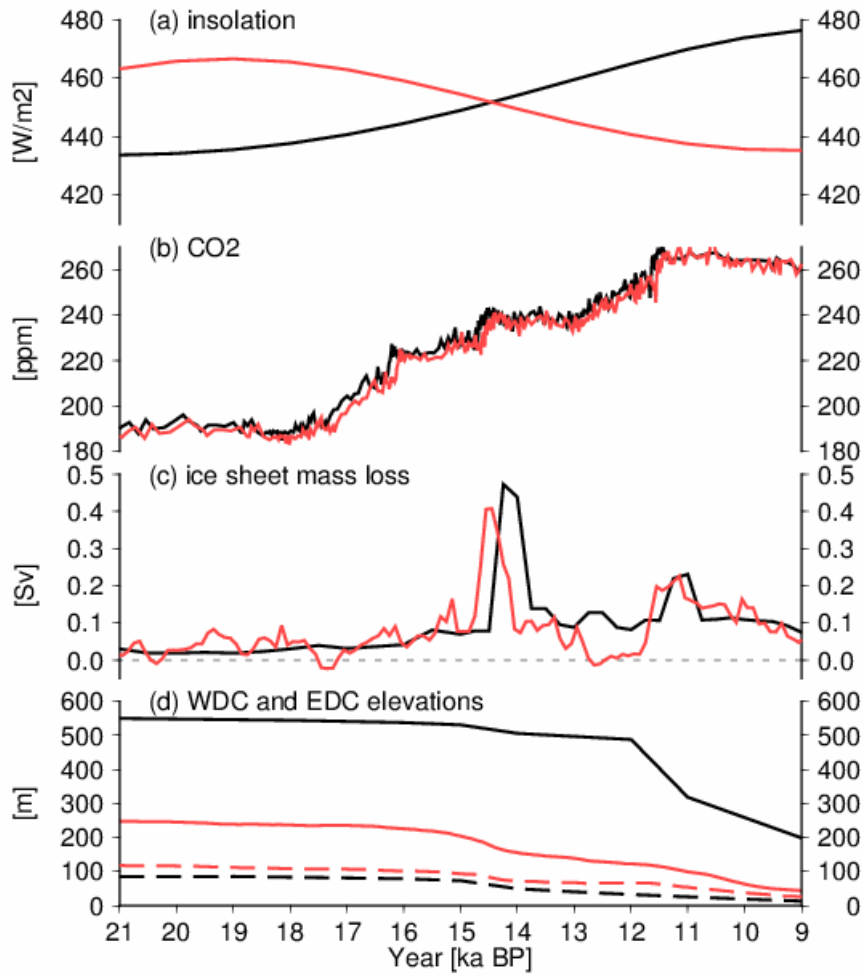
	CO ₂ coefficient [K/83 ppm]	AMOC coefficient [K/(normalised AMOC)]	Coefficient of Determination
iTRACE	6.5	−2.4	0.90
LOVECLIM	4.1	−0.4	0.91
MIROC	1.4	−0.5	0.81
HadCM3	3.3	−1.4	0.95

580 **Table 4:** Results of the MLR model for Southern Ocean SST.

MPI-ESM	3.1	−1.2	0.90
iLOVECLIM	1.0	−1.4	0.56

	CO ₂ coefficient [K/83 ppm]	AMOC coefficient [K/(normalised AMOC)]	Response timescale [year]	Coefficient of determination
iTRACE	6.0	−2.9	500	0.97
LOVECLIM	4.4	−0.6	300	0.94
MIROC	2.4	−0.9	600	0.97
HadCM3	4.8	−1.3	700	0.99
MPI-ESM	3.4	−1.4	500	0.95
iLOVECLIM	2.0	−0.8	100	0.54

581 **Table 5:** Results of the bipolar seesaw model for Southern Ocean SST



582

583 **Figure 1:** Forcing of the last deglaciation. (a) Insolation. Black: 65°N July, red: 65°S January based on
584 Berger (1978), (b) CO₂. Black: Bereiter et al., (2015), red: Kohler et al., (2017), (c) FWF in the NH from
585 ICE-6G_C (black lines) and GLAC-1D (red lines), (d-e) Elevation change at WDC (bold lines) and EDC
586 (dashed lines) from ICE-6G_C and GLAC-1D.

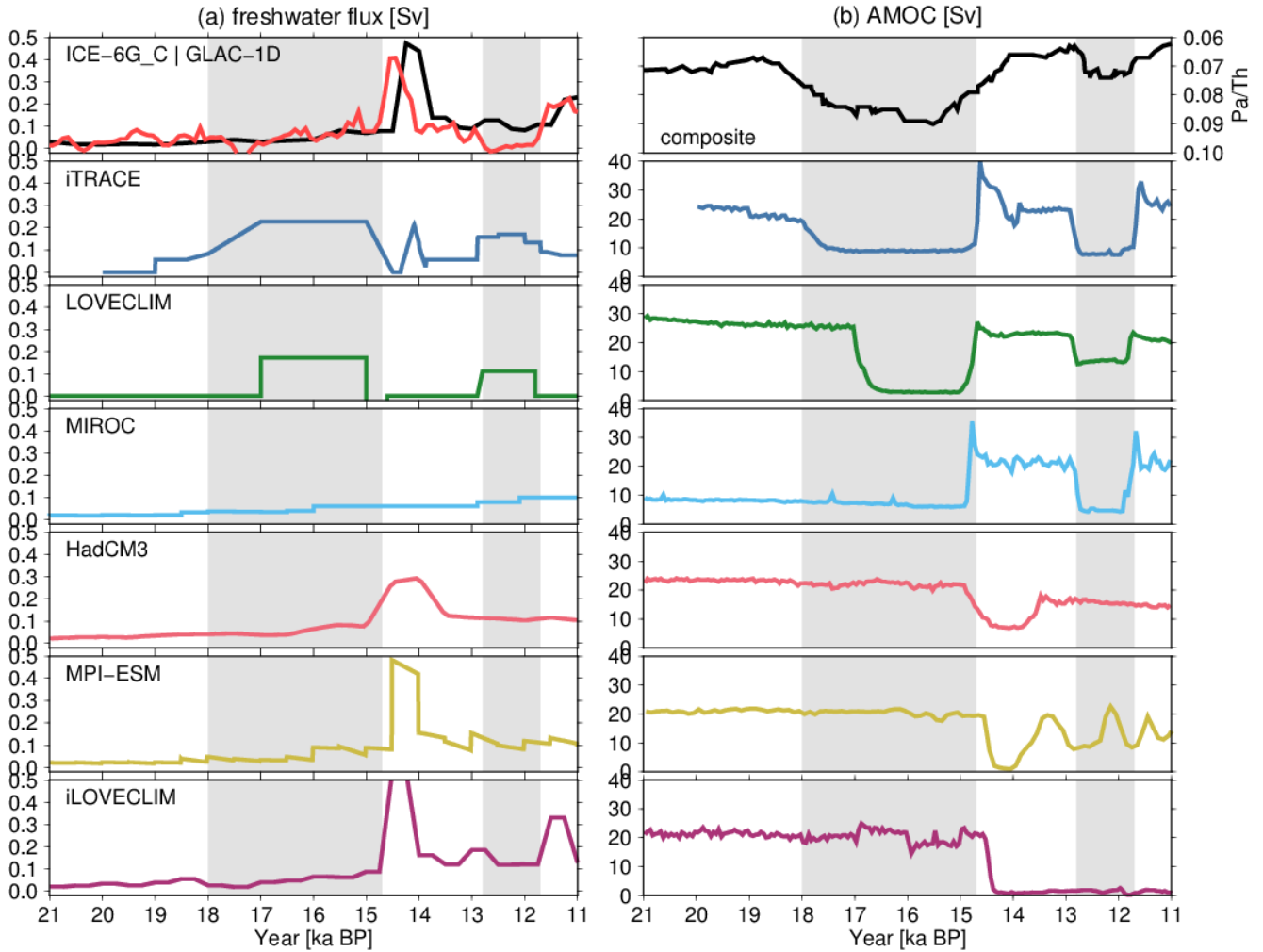


Figure 2: (a) Freshwater forcing (total value in the NH) and (b) simulated AMOC time series. The top panels indicate the freshwater flux from ice sheet reconstructions (black indicates ICE-6G_C and red indicates GLAC-1D) and composite $^{231}\text{Pa}/^{230}\text{Th}$ in the North Atlantic, retrieved from Ng et al., (2018). The grey shading indicates HS1 (18–14.7ka) and the YD (12.8–11.7ka), respectively, and the period in between corresponds to the BA (14.7–12.8 ka).

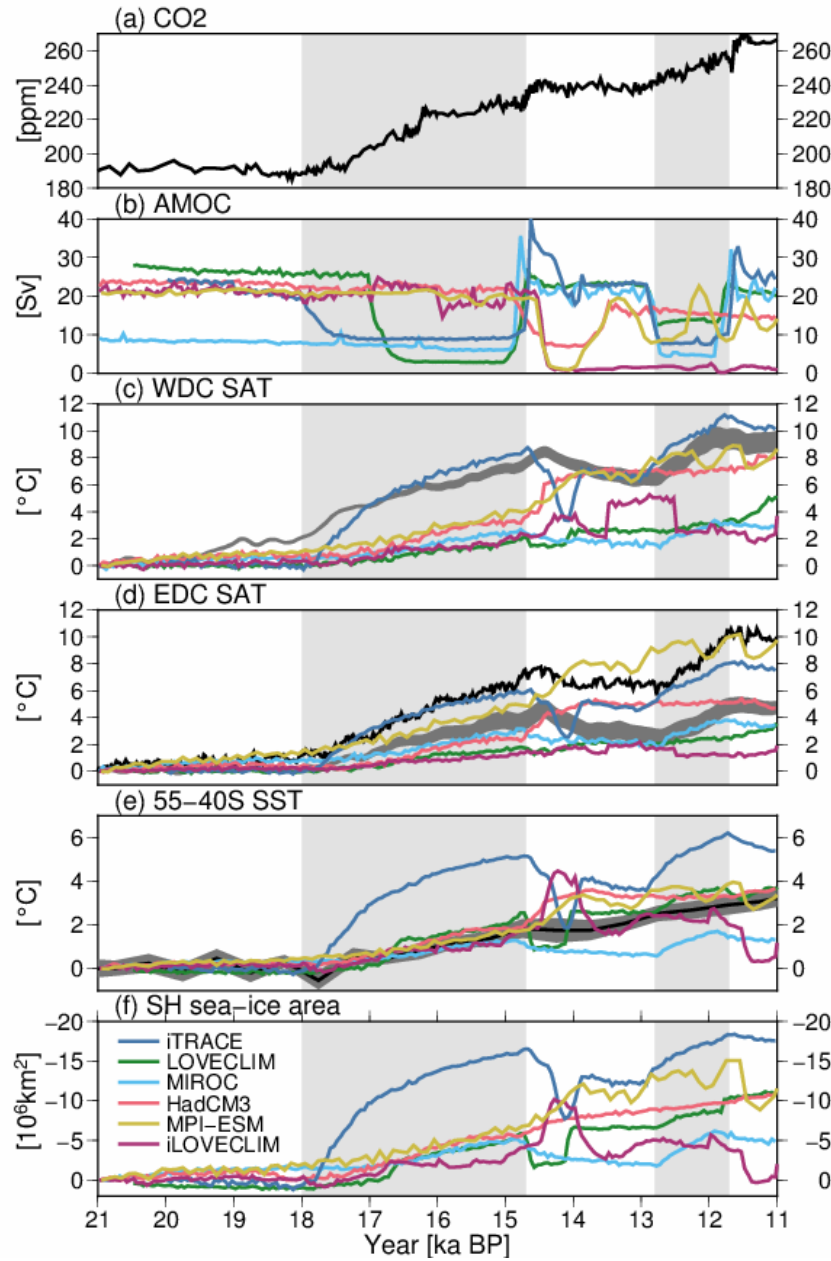


Figure 3: Time series of (a) atmospheric CO₂ (Bereiter et al., 2015) and (b) simulated AMOC, (c–d) SAT at WDC and EDC, (e) Southern Ocean SST, (f) Southern Ocean sea ice area in the transient simulations. The SAT, SST and sea ice area indicate changes since the LGM. The grey lines in (c–d) represent reconstructions from Buizert et al., (2013), and the black line in (d) represents reconstructions from Parrenin et al., (2013). The black lines and grey shades in (e) indicate the Southern Ocean SST stack and its standard error, respectively, as derived by Anderson et al., (2020).

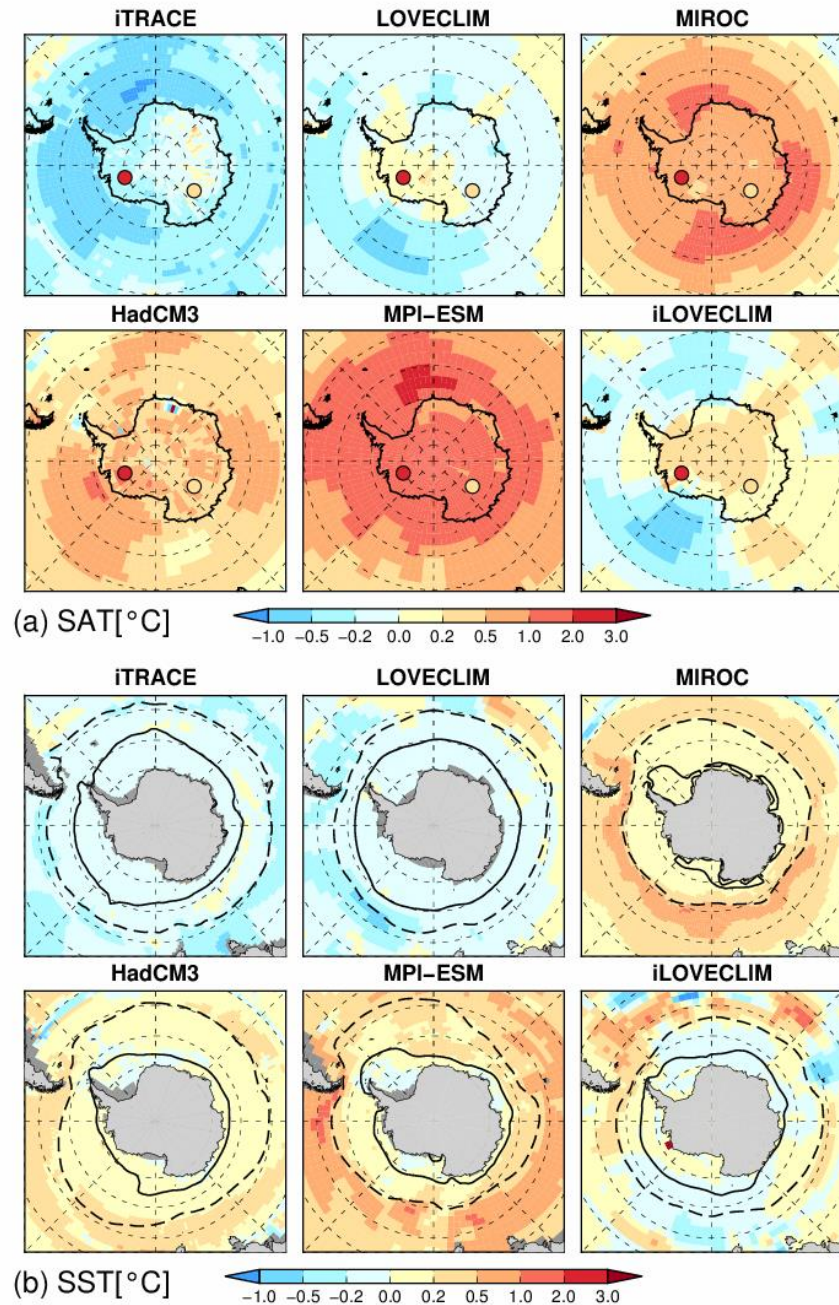


Figure 4: (a) SAT and (b) SST anomalies at 18 ka compared to the LGM. The coloured circles in (a) represent 18 ka-LGM SAT change based on ice core data (Parrenin et al., 2013), and the bold and dashed lines in (b) represent LGM austral summer and winter sea ice extent (85 and 15% annual-mean sea ice concentration), respectively.

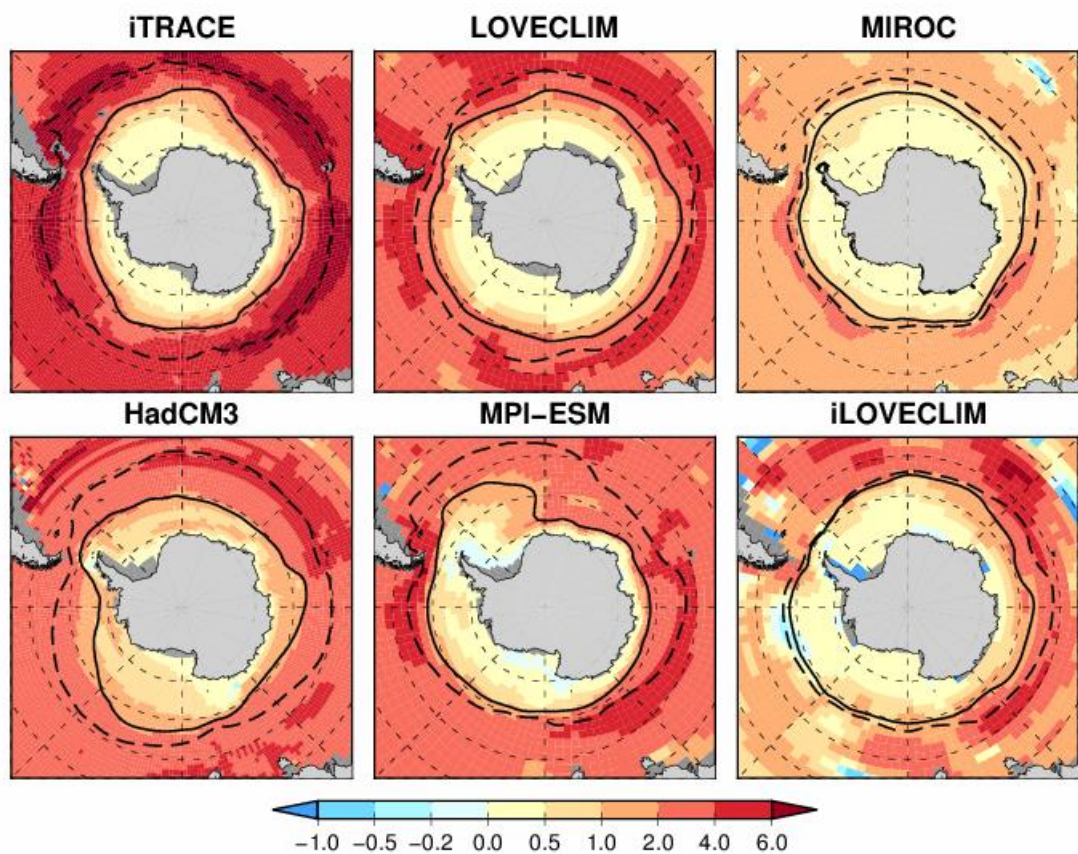


Figure 5: SST anomalies at 11 ka compared to the LGM. The bold and dashed lines indicate LGM and 11 ka sea ice extent (15% sea ice concentration), respectively.

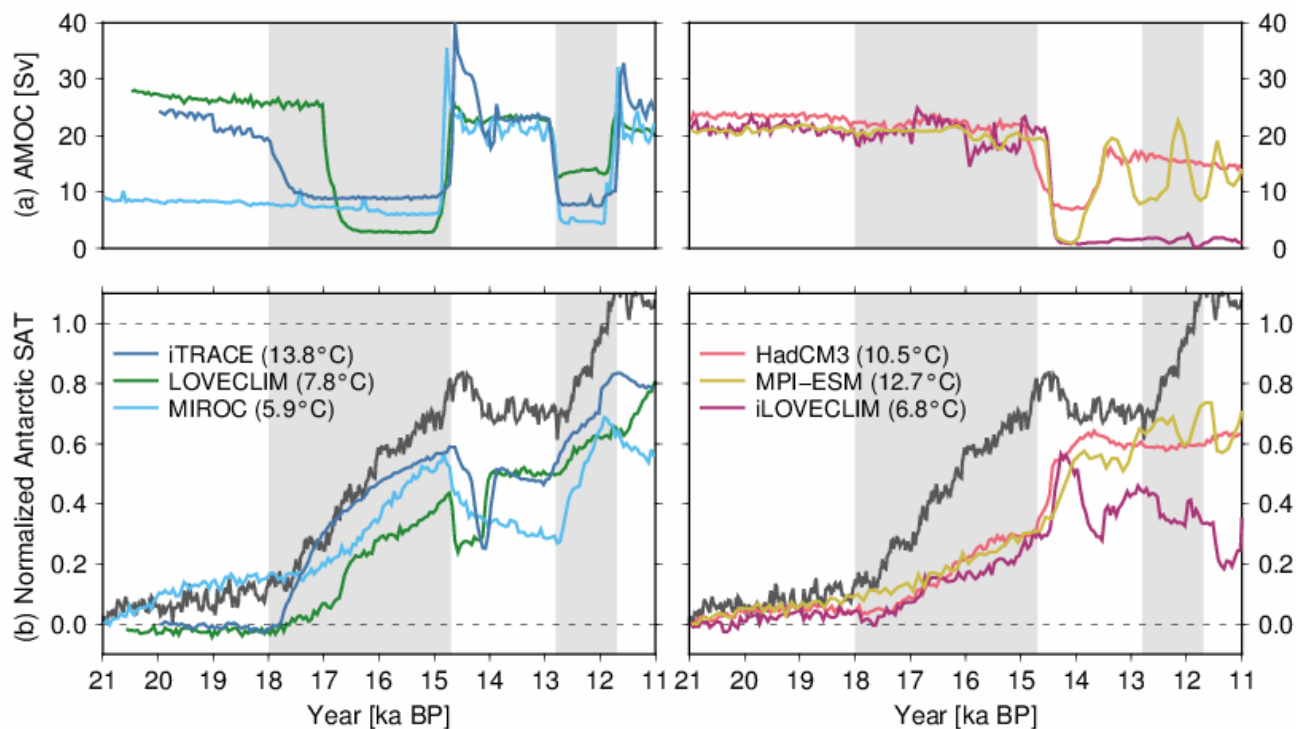
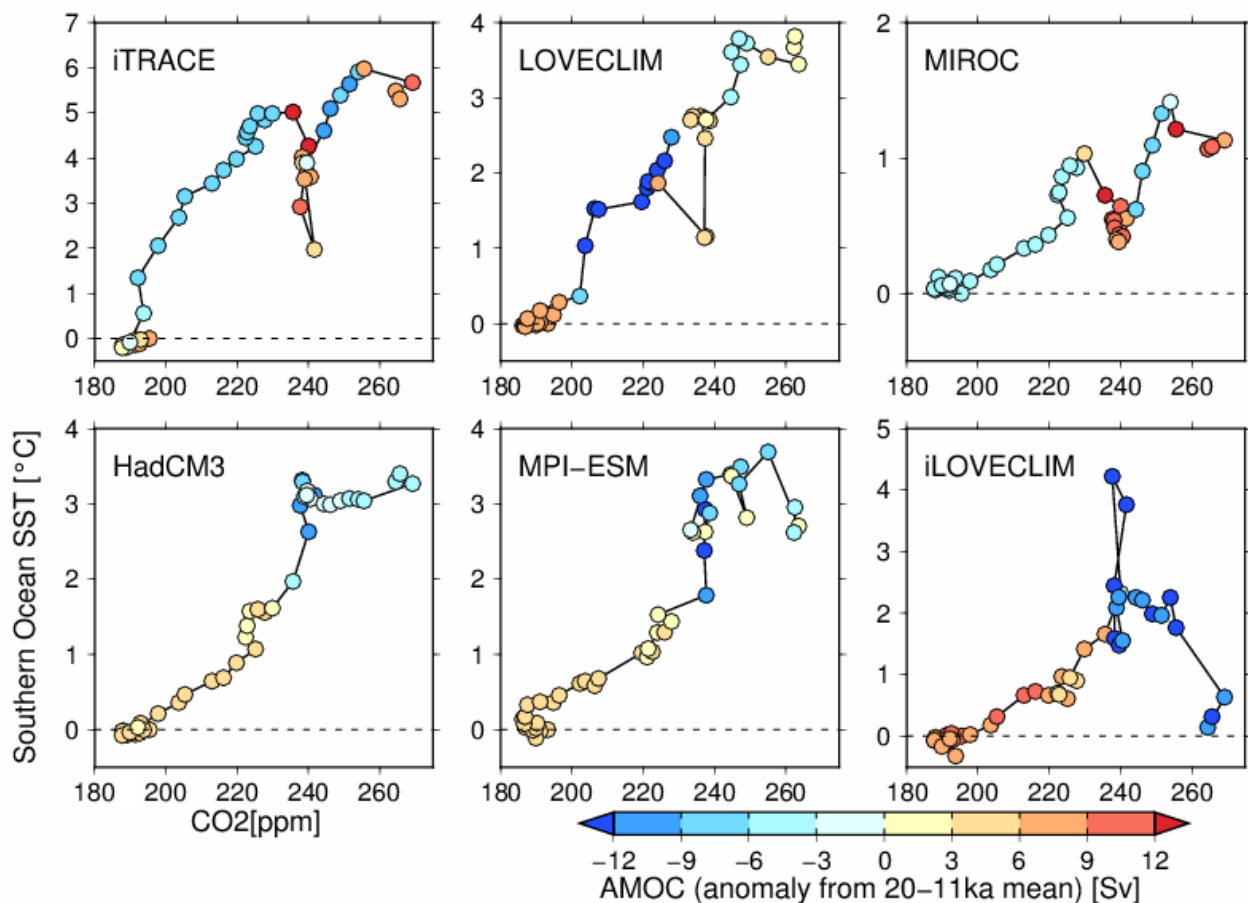


Figure 6: AMOC and normalised Antarctic SAT, with respect to the difference between PI and LGM. The actual PI and LGM differences are indicated in parentheses. The left panels show three simulations with weak AMOC during HS1, and the right show strong AMOC during HS1, respectively. The grey line in (b) is normalised Antarctic SAT from EDC based on Parrenin et al., 2013.



614

615 **Figure 7:** Relationship between Southern Ocean SST (vertical axis, change since LGM), CO₂ (horizontal
616 axis) and AMOC strength anomaly from the mean strength between 20–11 ka (colours). The trajectory
617 of the deglacial CO₂ forcing (CO₂), simulated SST changes and AMOC are plotted with circles at 200-
618 year intervals. Note that the vertical axes are different between models to represent the total deglacial
619 warming.

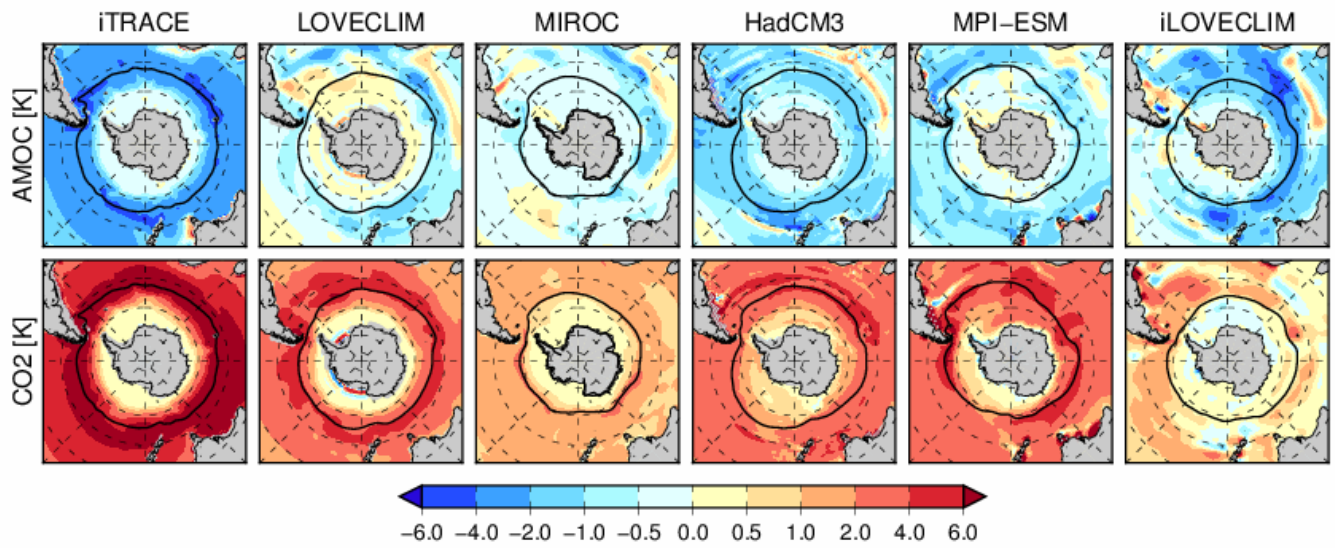


Figure 8: Results of the MLR model for 2-D SST maps. Top: AMOC coefficients. Bottom: CO₂ coefficients. The black lines represent LGM sea ice edges.

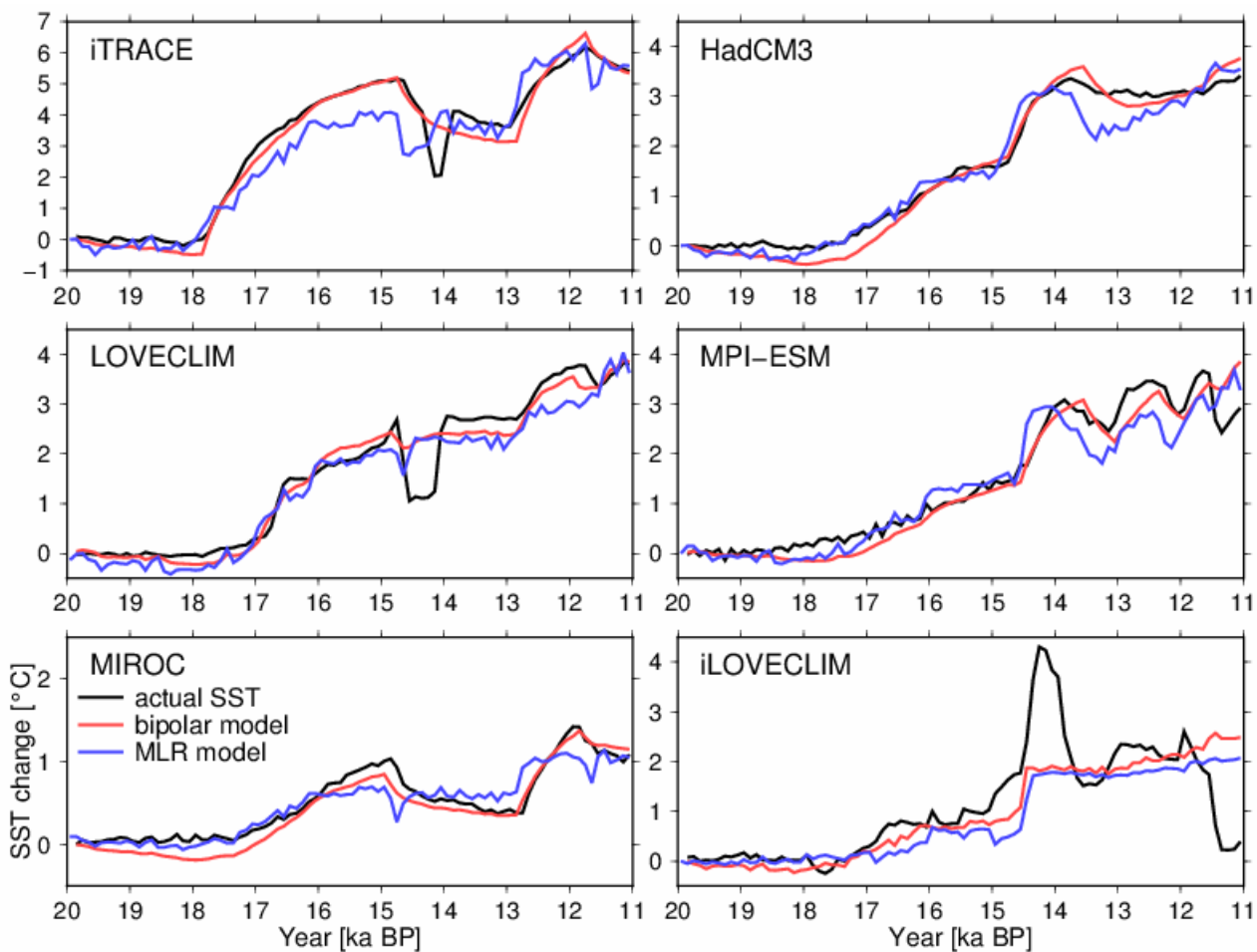


Figure 9: Results of the MLR model and bipolar seesaw model for Southern Ocean SST. The black lines represent the actual SST change (anomaly from 20 ka). The blue and red lines represent the results of MLR and bipolar seesaw models, respectively.

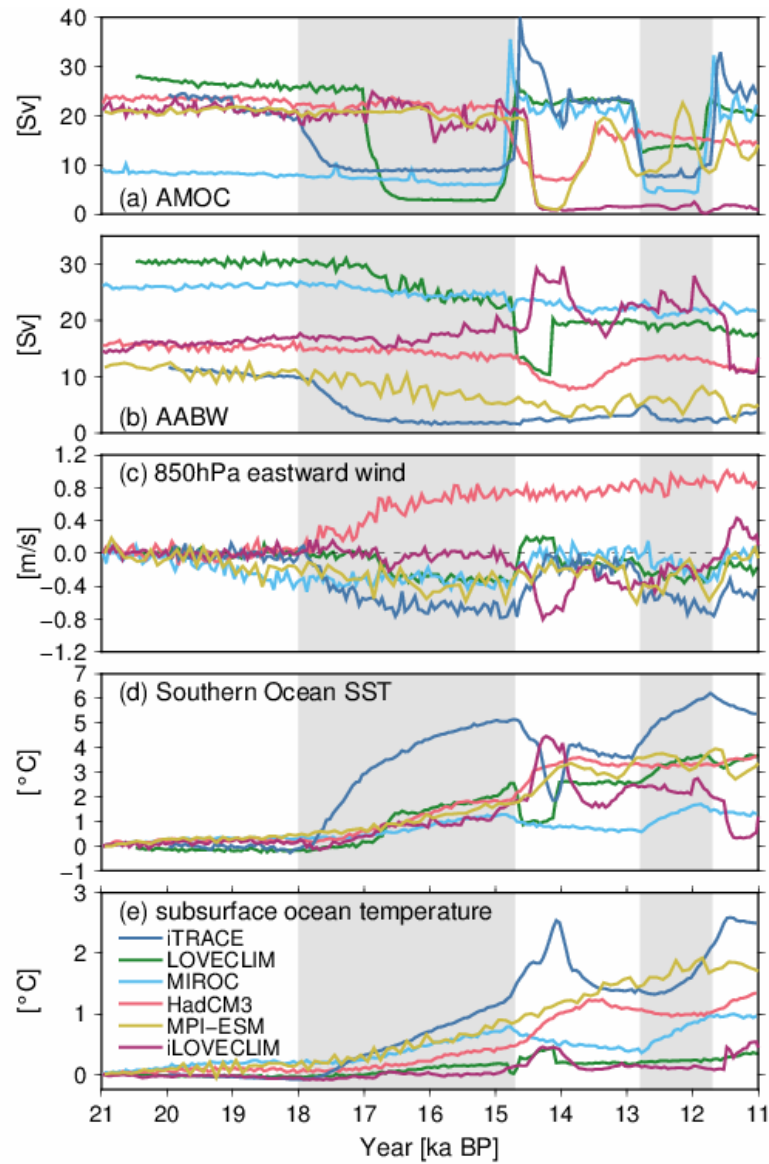


Figure 10: Time series of simulated (a) AMOC, (b) AABW, (c) 850hPa winds over the Southern Ocean (65–40°S), (d) Southern Ocean SST, and (e) subsurface ocean temperature south of 60°S (at depths 400–666m).

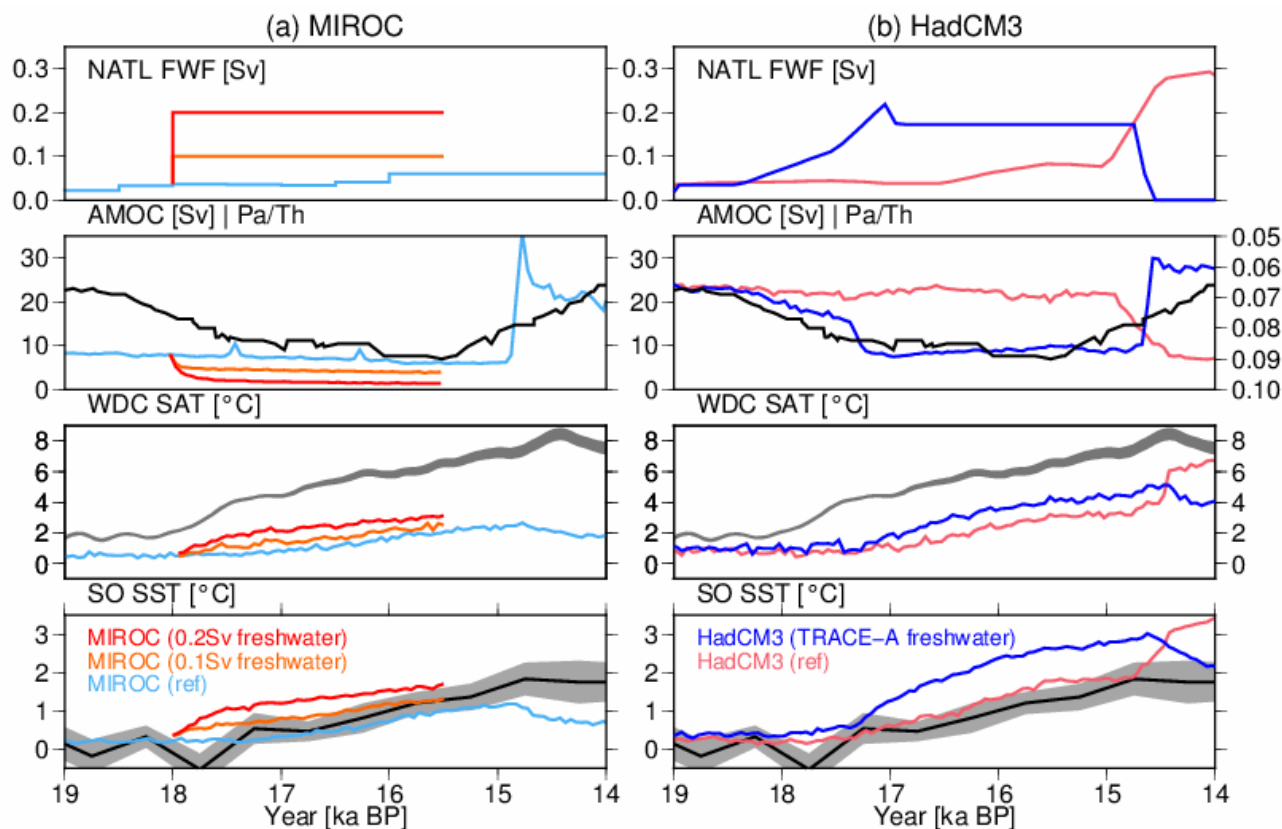


Figure 11: Results from transient deglaciation experiments performed with (a) MIROC and (b) HadCM3. The black lines in each panel represent the same proxy data as in Figure 3 (Parrenin et al., 2013; Buizert et al., 2021; Anderson et al., 2020). In two MIROC sensitivity experiments, a larger amount of freshwater flux (0.1 or 0.2 Sv) is added into the North Atlantic (50–70°N) during 18–15.5 ka compared to the standard MIROC experiment (light blue lines). In the TRACE-A HadCM3 sensitivity experiment (blue lines), a larger freshwater flux is added in the North Atlantic following the Trace-21ka simulation (Liu et al., 2009), while the pink lines in (b) represent the HadCM3 simulation used in Snoll et al. (2022).

References

1. Abe-Ouchi, A., Saito, F., Kawamura, K., Raymo, M. E., Okuno, J., Takahashi, K., and Blatter, H.: Insolation-driven 100,000-year glacial cycles and hysteresis of ice-sheet volume. *Nature* 500, 190–193, doi: 10.1038/nature12374, 2013
2. Anderson, B. E., & Burckle, L. H.: Rise in Atmospheric CO₂. *Science*, 323 (March), 1443–1448, 2009

- 648 3. Anderson, H. J., Pedro, J. B., Bostock, H. C., Chase, Z., and Noble, T. L.: Compiled Southern Ocean
649 sea surface temperatures correlate with Antarctic Isotope Maxima, *Quaternary Science Reviews*, 255,
650 106821, <https://doi.org/10.1016/j.quascirev.2021.106821>, 2021.
- 651 4. Anderson, Harris J; Pedro, Joel B; Bostock, Helen C; Chase, Zanna; Noble, Taryn L (2020): Southern
652 Ocean Sea Surface Temperature Anomaly Stacks [dataset]. PANGAEA,
653 <https://doi.org/10.1594/PANGAEA.912158>
- 654 5. Annan, J. D., Hargreaves, J. C., and Mauritsen, T.: A new global surface temperature reconstruction
655 for the Last Glacial Maximum, *Clim. Past*, 18, 1883–1896, <https://doi.org/10.5194/cp-18-1883-2022>,
656 2022.
- 657 6. Bentley, M. J., Ocofaigh, C., Anderson, J. B., Conway, H., Davies, B., Graham, A. G. C., Hillenbrand,
658 C. D., Hodgson, D. A., Jamieson, S. S. R., Larter, R. D., Mackintosh, A., Smith, J. A., Verleyen, E.,
659 Ackert, R. P., Bart, P. J., Berg, S., Brunstein, D., Canals, M., Colhoun, E. A., Crosta, X., Dickens,
660 W. A., Domack, E., Dowdeswell, J. A., Dunbar, R., Ehrmann, W., Evans, J., Favier, V., Fink, D.,
661 Fogwill, C. J., Glasser, N. F., Gohl, K., Golledge, N. R., Goodwin, I., Gore, D. B., Greenwood, S. L.,
662 Hall, B. L., Hall, K., Hedding, D. W., Hein, A. S., Hocking, E. P., Jakobsson, M., Johnson, J. S.,
663 Jomelli, V., Jones, R. S., Klages, J. P., Kristoffersen, Y., Kuhn, G., Leventer, A., Licht, K., Lilly, K.,
664 Lindow, J., Livingstone, S. J., Massé, G., McGlone, M. S., McKay, R. M., Melles, M., Miura, H.,
665 Mulvaney, R., Nel, W., Nitsche, F. O., O'Brien, P. E., Post, A. L., Roberts, S. J., Saunders, K. M.,
666 Selkirk, P. M., Simms, A. R., Spiegel, C., Stollendorf, T. D., Sugden, D. E., van der Putten, N., van
667 Ommen, T., Verfaillie, D., Vyverman, W., Wagner, B., White, D. A., Witus, A. E., and Zwart, D.:
668 A community-based geological reconstruction of Antarctic Ice Sheet deglaciation since the Last
669 Glacial Maximum, *Quaternary Sci. Rev.*, 100, 1–9, <https://doi.org/10.1016/j.quascirev.2014.06.025>,
670 2014.
- 671 7. Berger, A.: Long-Term Variations of Daily Insolation and Quaternary Climatic Changes, *J. Atmos.*
672 *Sci.*, 35, 2362–2367, doi:10.1175/1520-0469(1978)035<2362:LTVODI>2.0.CO;2, 1978.
- 673 8. Bereiter, B., Eggleston, S., Schmitt, J., Nehrbass-Ahles, C., Stocker, T. F., Fischer, H., Kipfstuhl, S.,
674 and Chappellaz, J.: Revision of the EPICA Dome C CO₂ record from 800 to 600 kyr before present,
675 *Geophys. Res. Lett.*, 42, 542–549, 10.1002/2014GL061957, 2015.

- 676 9. Bereiter, B., Shackleton, S., Baggenstos, D., Kawamura, K., and Severinghaus, J.: Mean global ocean
677 temperatures during the last glacial transition. *Nature*, 553(7686), 39–44.
678 <https://doi.org/10.1038/nature25152>, 2018.
- 679 10. Bethke, I., Li, C., and Nisancioglu, K. H.: Can we use ice sheet reconstructions to constrain meltwater
680 for deglacial simulations? *Paleoceanography*, 27 (November 2011), 1–17.
681 doi:10.1029/2011PA002258, 2012
- 682 11. Böhm, E., Lippold, J., Gutjahr, M., Frank, M., Blaser, P., Antz, B., Fohlmeister, J., Frank, N.,
683 Andersen, M. B. and Deininger, M.: Strong and deep Atlantic meridional overturning circulation
684 during the last glacial cycle. *Nature*, 517(7534), 73–76. <https://doi.org/10.1038/nature14059>, 2015.
- 685 12. Bouttes, N., Roche, D. M., and Paillard, D.: Systematic study of the impact of fresh water fluxes on
686 the glacial carbon cycle, *Clim. Past*, 8, 589–607, <https://doi.org/10.5194/cp-8-589-2012>, 2012.
- 687 13. Bouttes, N., Lhardy, F., Quiquet, A., Paillard, D., Goosse, H., and Roche, D. M.: Deglacial climate
688 changes as forced by different ice sheet reconstructions, *Clim. Past*, 19, 1027–1042,
689 <https://doi.org/10.5194/cp-19-1027-2023>, 2023.
- 690 14. Buizert, C., Gkinis, V., Severinghaus, J. P., He, F., Lecavalier, B. S., Kindler, P., Leuenberger, M.,
691 Carlson, A. E., Vinther, B., Masson-Delmotte, V., White, J. W. C., Liu, Z., Otto-Bliesner, B., and
692 Brook, E. J.: Greenland temperature response to climate forcing during the last deglaciation, *Science*,
693 345, 1177–1180, [10.1126/science.1254961](https://doi.org/10.1126/science.1254961), 2014.
- 694 15. Buizert, C., Fudge, T. J., Roberts, W. H., Steig, E. J., Sherriff-Tadano, S., Ritz, C., Lefebvre, E.,
695 Edwards, J., Kawamura, K., Oyabu, I., Motoyama, H. Kahle, E. C., Jones, T. R., Abe-ouchi, A.,
696 Obase, T., Martin, C., Corr, H., Severinghaus, J. P., Beaudette, R. Epifanio, J. A., Brook, E. J., Martin,
697 K., Aoki, S., Nakazawa, T., Sowers, T. A., Alley, R. B., Ahn, J., Sigl, M., Severi, M., Dunbar, N. W.,
698 Svensson, A., Fegyveresi, J. M., He, C., Liu, Z., Zhu, J., Otto-bliesner, B. L., Lipenkov, V. Y.,
699 Kageyama, M., and Schwander, J.: Antarctic surface temperature and elevation during the Last
700 Glacial Maximum, *Science* 372(6546), 1097–1101, doi: 10.1126/science.abd2897, 2021
- 701 16. Burke, A. and Robinson, L. F.: The Southern Ocean’s Role in Carbon Exchange During the Last
702 Deglaciation, *Science*, 135, 6068, 557–561. <https://doi.org/10.1126/science.1208163>, 2011

17. Capron, E., Landais, A., Chappellaz, J., Schilt, A., Buiron, D., Dahl-Jensen, D., Johnsen, S. J., Jouzel, J., Lemieux-Dudon, B., Loulergue, L., Leuenberger, M., Masson-Delmotte, V., Meyer, H., Oerter, H., and Stenni, B.: Millennial and sub-millennial scale climatic variations recorded in polar ice cores over the last glacial period, *Clim. Past*, 6, 345–365, <https://doi.org/10.5194/cp-6-345-2010>, 2010.
18. Chan, W.-L. and Abe-Ouchi, A.: Pliocene Model Intercomparison Project (PlioMIP2) simulations using the Model for Interdisciplinary Research on Climate (MIROC4m), *Clim. Past*, 16, 1523–1545, <https://doi.org/10.5194/cp-16-1523-2020>, 2020.
19. Clark, P. U., He, F., Golledge, N. R., Mitrovica, J. X., Dutton, A., Hoffman, J. S., and Dendy, S.: Oceanic forcing of penultimate deglacial and last interglacial sea-level rise. *Nature*, 577(7792), 660–664. <https://doi.org/10.1038/s41586-020-1931-7>, 2020
20. Condron, A., & Winsor, P.: Meltwater routing and the Younger Dryas. *Proceedings of the National Academy of Sciences*, 109(49), 19928–19933, <https://doi.org/10.1073/pnas.1207381109>, 2012
21. Crosta, X., Kohfeld, K. E., Bostock, H. C., Chadwick, M., Du Vivier, A., Esper, O., Etourneau, J., Jones, J., Leventer, A., Müller, J., Rhodes, R. H., Allen, C. S., Ghadi, P., Lamping, N., Lange, C. B., Lawler, K.-A., Lund, D., Marzocchi, A., Meissner, K. J., Meniel, L., Nair, A., Patterson, M., Pike, J., Prebble, J. G., Riesselman, C., Sadatzki, H., Sime, L. C., Shukla, S. K., Thöle, L., Vorrath, M.-E., Xiao, W., and Yang, J.: Antarctic sea ice over the past 130 000 years – Part 1: a review of what proxy records tell us, *Clim. Past*, 18, 1729–1756, <https://doi.org/10.5194/cp-18-1729-2022>, 2022.
22. Dansgaard, W., Johnsen, S. J., Clausen, H. B., Dahl-Jensen, D., Gundestrup, N. S., Hammer, C. U., Hvidberg, C. S., Steffensen, J. P., Sveinbjörnsdottir, A. E., Jouzel, J., and Bond, G.: Evidence for general instability of past climate from a 250-kyr ice-core record, *Nature*, 364, 218–220, <https://doi.org/10.1038/364218a0>, 1993
23. Deschamps, P., Durand, N., Bard, E., Hamelin, B., Camoin, G., Thomas, A. L., Henderson, G. M., Okuno, J., and Yokoyama, Y.: Ice-sheet collapse and sea-level rise at the Bølling warming 14,600 years ago, *Nature*, 28, 559–564, <https://doi.org/10.1038/nature10902>, 2012.
24. Golledge, N., Meniel, L., Carter, L., Fogwill, C. J., England, M. H., Cortese, G., and Levy, R. H.: Antarctic contribution to meltwater pulse 1A from reduced Southern Ocean overturning. *Nat Commun* 5, 5107, <https://doi.org/10.1038/ncomms6107>, 2014.

- 731 25. Gomez, N., Weber, M. E., Clark, P. U., Mitrovica, J. X. and Han, H. K.: Antarctic ice dynamics
732 amplified by Northern Hemisphere sea-level forcing, *Nature*, 587(7835), 600–604,
733 doi:10.1038/s41586-020-2916-2, 2020
- 734 26. Goosse, H., Brovkin, V., Fichefet, T., Haarsma, R., Huybrechts, P., Jongma, J., Mouchet, A., Selten,
735 F., Barriat, P.-Y., Campin, J.-M., Deleersnijder, E., Driesschaert, E., Goelzer, H., Janssens, I., Loutre,
736 M.-F., Morales Maqueda, M. A., Opsteegh, T., Mathieu, P.-P., Munhoven, G., Pettersson, E. J.,
737 Renssen, H., Roche, D. M., Schaeffer, M., Tartinville, B., Timmermann, A., and Weber, S. L.:
738 Description of the Earth system model of intermediate complexity LOVECLIM version 1.2, *Geosci.*
739 *Model Dev.*, 3, 603–633, <https://doi.org/10.5194/gmd-3-603-2010>, 2010.
- 740 27. Gottschalk, J., Battaglia, G., Fischer, H., Frölicher, T. L., Jaccard, S. L., Jeltsch-Thömmes, A., Joos,
741 F., Köhler, P., Meissner, K. J., Menviel, L., Nehrbass-Ahles, C., Schmitt, J., Schmittner, A., Skinner,
742 L. C., and Stocker, T. F.: Mechanisms of millennial-scale atmospheric CO₂ change in numerical
743 model simulations, *Quaternary Sci. Rev.*, 220, 30–74,
744 <https://doi.org/10.1016/j.quascirev.2019.05.013>, 2019.
- 745 28. Gray, W. R., de Lavergne, C., Willis, R. C. J., Menviel, L., Spence, P., Holzer, M., Kageyama, M.
746 and Michel, E.: Poleward Shift in the Southern Hemisphere Westerly Winds Synchronous With the
747 Deglacial Rise in CO₂, *Paleoceanography and Paleoclimatology*, 38, 7,
748 <https://doi.org/10.1029/2023PA004666>, 2023
- 749 29. Green, R. A., Menviel, L., Meissner, K. J., Crosta, X., Chandan, D., Lohmann, G., Peltier, W. R., Shi,
750 X., and Zhu, J.: Evaluating seasonal sea-ice cover over the Southern Ocean at the Last Glacial
751 Maximum, *Clim. Past*, 18, 845–862, <https://doi.org/10.5194/cp-18-845-2022>, 2022.
- 752 30. Gregoire, L. J., Payne, A. J., and Valdes, P. J.: Deglacial rapid sea level rises caused by ice-sheet
753 saddle collapses, *Nature*, 487, 219–222, 10.1038/nature11257, 2012.
- 754 31. He, F., Shakun, J. D., Clark, P. U., Carlson, A. E., Liu, Z., Otto-Bliesner, B. L., and Kutzbach, J. E.:
755 Northern Hemisphere forcing of Southern Hemisphere climate during the last deglaciation, *Nature*,
756 494, 81–85, <https://doi.org/10.1038/nature11822>, 2013.

32. He, C., Zhengyu Liu, and Aixue Hu.: The transient response of atmospheric and oceanic heat transports to anthropogenic warming. *Nature Climate Change*, 1, doi:10.1038/s41558-018-0387-3, 2019.
33. He, C., Liu, Z., Zhu, J., Zhang, J., Gu, S., Otto-Bliesner, B. L., Brady, E., Zhu, C., Jin, Y. and Sun, J.: North Atlantic subsurface temperature response controlled by effective freshwater input in “Heinrich” events, *Earth and Planetary Science Letters*, 539, 116247, <https://doi.org/10.1016/j.epsl.2020.116247>, 2020.
34. He, C., Liu, Z., Otto-Bliesner, B. L., Brady, E. C., Zhu, C., Tomas, R., Bao, Y.: Hydroclimate footprint of pan-Asian monsoon water isotope during the last deglaciation. *Science Advances*, 7(4), 1–12. <https://doi.org/10.1126/sciadv.abe2611>, 2021.
35. Hunter, S. J., Haywood, A. M., Dolan, A. M., and Tindall, J. C.: The HadCM3 contribution to PlioMIP phase 2, *Clim. Past*, 15, 1691–1713, <https://doi.org/10.5194/cp-15-1691-2019>, 2019.
36. Ivanovic, R. F., Gregoire, L. J., Kageyama, M., Roche, D. M., Valdes, P. J., Burke, A., Drummond, R., Peltier, W. R., and Tarasov, L.: Transient climate simulations of the deglaciation 21–9 thousand years before present (version 1) – PMIP4 Core experiment design and boundary conditions, *Geosci. Model Dev.*, 9, 2563–2587, <https://doi.org/10.5194/gmd-9-2563-2016>, 2016.
37. Ivanovic, R. F., Gregoire, L. J., Burke, A., Wickert, A. D., and Valdes, P. J.: Acceleration of Northern Ice Sheet Melt Induces AMOC Slowdown and Northern Cooling in Simulations of the Early Last Deglaciation, *Paleoceanography and Paleoclimatology*. 807–824. doi:10.1029/2017PA003308, 2018
38. Jouzel, J., Masson-Delmotte, V., Cattani, O., Dreyfus, G., Falourd, S., Hoffmann, G., Minster, B., Nouet, J., Barnola, J. M., Chappellaz, J., Fischer, H., Gallet, J. C., Johnsen, S., Leuenberger, M., Loulergue, L., Luethi, D., Oerter, H., Parrenin, F., Raisbeck, G., Raynaud, D., Schilt, A., Schwander, J., Selmo, E., Souchez, R., Spahni, R., Stauffer, B., Steffensen, J. P., Stenni, B., Stocker, T. F., Tison, J. L., Werner, M., and Wolff, E. W.: Orbital and Millennial Antarctic Climate Variability over the Past 800,000 Years, *Science*, 317, 793-796, <https://doi.org/10.1126/science.1141038>, 2007.
39. Kageyama, M., Merkel, U., Otto-Bliesner, B., Prange, M., Abe-Ouchi, A., Lohmann, G., Ohgaito, R., Roche, D. M., Singarayer, J., Swingedouw, D., and X Zhang: Climatic impacts of fresh water

hosing under Last Glacial Maximum conditions: a multi-model study, *Clim. Past*, 9, 935–953, <https://doi.org/10.5194/cp-9-935-2013>, 2013.

40. Kageyama, M., Braconnot, P., Harrison, S. P., Haywood, A. M., Jungclaus, J. H., Otto-Bliesner, B. L., Peterschmitt, J.-Y., Abe-Ouchi, A., Albani, S., Bartlein, P. J., Brierley, C., Crucifix, M., Dolan, A., Fernandez-Donado, L., Fischer, H., Hopcroft, P. O., Ivanovic, R. F., Lambert, F., Lunt, D. J., Mahowald, N. M., Peltier, W. R., Phipps, S. J., Roche, D. M., Schmidt, G. A., Tarasov, L., Valdes, P. J., Zhang, Q., and Zhou, T.: The PMIP4 contribution to CMIP6 – Part 1: Overview and overarching analysis plan, *Geosci. Model Dev.*, 11, 1033–1057, <https://doi.org/10.5194/gmd-11-1033-2018>, 2018.
41. Kageyama, M., Harrison, S. P., Kapsch, M.-L., Lofverstrom, M., Lora, J. M., Mikolajewicz, U., Sherriff-Tadano, S., Vadsaria, T., Abe-Ouchi, A., Bouttes, N., Chandan, D., Gregoire, L. J., Ivanovic, R. F., Izumi, K., LeGrande, A. N., Lhardy, F., Lohmann, G., Morozova, P. A., Ohgaito, R., Paul, A., Peltier, W. R., Poulsen, C. J., Quiquet, A., Roche, D. M., Shi, X., Tierney, J. E., Valdes, P. J., Volodin, E., and Zhu, J.: The PMIP4 Last Glacial Maximum experiments: preliminary results and comparison with the PMIP3 simulations, *Clim. Past*, 17, 1065–1089, <https://doi.org/10.5194/cp-17-1065-2021>, 2021.
42. Kapsch, M.-L., Mikolajewicz, U., Ziemen, F. and Schannwell, C.: Ocean response in transient simulations of the last deglaciation dominated by underlying ice-sheet reconstruction and method of meltwater distribution, *Geophysical Research Letters*, 49, e2021GL096767, <https://doi.org/10.1029/2021GL096767>, 2022.
43. Kobayashi, H., Oka, A., Yamamoto, A., and Abe-Ouchi, A.: Glacial carbon cycle changes by Southern Ocean processes with sedimentary amplification. *Science Advances*, 7(35), doi: 10.1126/sciadv.abg7723, 2021.
44. Kobayashi, H., Oka, A., Obase, T., and Abe-Ouchi, A.: Assessing transient changes in the ocean carbon cycle during the last deglaciation through carbon isotope modeling, *Clim. Past*, 20, 769–787, <https://doi.org/10.5194/cp-20-769-2024>, 2024.

- 810 45. Kuniyoshi, Y., Abe-Ouchi, A., Sherriff-Tadano, S., Chan, W.-L., and Saito, F.: Effect of Climatic
811 Precession on Dansgaard-Oeschger-Like Oscillations. *Geophysical Research Letters*, 49(6),
812 e2021GL095695. <https://doi.org/10.1029/2021GL095695>, 2022.
- 813 46. Lambeck, K., Rouby, H., Purcell, A., Sun, Y., and Sambridge, M.: Sea level and global ice volumes
814 from the Last Glacial Maximum to the Holocene, *P. Natl. Acad. Sci.*, 111, 15296–15303,
815 10.1073/pnas.1411762111, 2014.
- 816 47. Lhardy, F., Bouttes, N., Roche, D. M., Crosta, X., Waelbroeck, C., and Paillard, D.: Impact of
817 Southern Ocean surface conditions on deep ocean circulation during the LGM: a model analysis,
818 *Clim. Past*, 17, 1139–1159, <https://doi.org/10.5194/cp-17-1139-2021>, 2021.
- 819 48. Lisiecki, L. E. and Raymo, M. E.: A Pliocene-Pleistocene stack of 57 globally distributed benthic
820 $\delta^{18}\text{O}$ records, *Paleoceanography*, 20, PA1003, doi:10.1029/2004PA001071, 2005
- 821 49. Liu, Z., Otto-Bliesner, B. L., He, F., Brady, E. C., Tomas, R., Clark, P. U., Carlson, A. E., Lynch-
822 Stieglitz, J., Curry, W., Brook, E., Erickson, D., Jacob, R., Kutzbach, J., and Cheng, J.: Transient
823 Simulation of Last Deglaciation with a New Mechanism for Bølling-Allerød Warming, *Science*, 325,
824 310–314, doi:10.1126/science.1171041, 2009
- 825 50. Liu, Z., Bao, Y., Thompson, L. G., Mosley-Thompson, E., Tabor, C., Zhang, G. J., Yan, M.,
826 Lofverstrom, M., Montanez, I., and Oster, J.: Tropical mountain ice core $\delta^{18}\text{O}$: A Goldilocks
827 indicator for global temperature change, *Science Advances*, 9, 45,
828 <https://doi.org/10.1126/sciadv.adi6725>, 2023
- 829 51. Love, R., Andres, H. J., Condron, A., and Tarasov, L.: Freshwater routing in eddy-permitting
830 simulations of the last deglacial: the impact of realistic freshwater discharge, *Clim. Past*, 17, 2327–
831 2341, <https://doi.org/10.5194/cp-17-2327-2021>, 2021.
- 832 52. Lowry, D. P., Golledge, N. R., Menviel, L., and Bertler, N. A. N.: Deglacial evolution of regional
833 Antarctic climate and Southern Ocean conditions in transient climate simulations. 189–215, 2018.
- 834 53. Lynch-Stieglitz, J., Adkins, J. F., Curry, W. B., Dokken, T., Hall, I. R., Herguera, J. C. and Zahn, R.:
835 Atlantic meridional overturning circulation during the Last Glacial Maximum. *Science*, 316(5821),
836 66–69. <https://doi.org/10.1126/science.1137127>, 2007

- 837 54. MacDougall, A. H., Frölicher, T. L., Jones, C. D., Rogelj, J., Matthews, H. D., Zickfeld, K., Arora,
838 V. K., Barrett, N. J., Brovkin, V., Burger, F. A., Eby, M., Eliseev, A. V., Hajima, T., Holden, P. B.,
839 Jeltsch-Thömmes, A., Koven, C., Mengis, N., Menviel, L., Michou, M., Mokhov, I. I., Oka, A.,
840 Schwinger, J., Séférian, R., Shaffer, G., Sokolov, A., Tachiiri, K., Tjiputra, J., Wiltshire, A., and
841 Ziehn, T.: Is there warming in the pipeline? A multi-model analysis of the Zero Emissions
842 Commitment from CO₂, *Biogeosciences*, 17, 2987–3016, <https://doi.org/10.5194/bg-17-2987-2020>,
843 2020.
- 844 55. Marcott, S. A., Bauska, T. K., Buizert, C., Steig, E. J., Rosen, J. L., Cuffey, K. M., Fudge, T. J.,
845 Severinghaus, J. P., Kalk, M. L., McConnell, J. R., Sowers, T., Taylor, K. C. White, J. W. C. and
846 Brook, E. J.: Centennial-scale changes in the global carbon cycle during the last deglaciation. *Nature*,
847 514(7524), 616–619. <https://doi.org/10.1038/nature13799>, 2014
- 848 56. Margari, V., Skinner, L. C., Menviel, L., Capron, E., Rhodes, R. H., Martrat, B., and Grimalt, J. O.:
849 Fast and slow components of interstadial warming in the North Atlantic during the last glacial.
850 *Communications Earth & Environment*, 1–9. <https://doi.org/10.1038/s43247-020-0006-x>, 2020
- 851 57. Mariotti, V., Paillard, D., Bopp, L., Roche, D. M., and Bouttes, N.: A coupled model for carbon and
852 radiocarbon evolution during the last deglaciation. *Geophysical Research Letters*, 43(3), 1306–1313.
853 <https://doi.org/10.1002/2015GL067489>, 2016.
- 854 58. Marson, J. M., Mysak, L. A., Mata, M. M., and Wainer, I.: Evolution of the deep Atlantic water
855 masses since the last glacial maximum based on a transient run of NCAR-CCSM3. *Climate Dynamics*,
856 47(3–4), 865–877. <https://doi.org/10.1007/s00382-015-2876-7>, 2016
- 857 59. Martínez-García, A., Rosell-Melé, A., Jaccard, S.: Southern Ocean dust–climate coupling over the
858 past four million years. *Nature* 476, 312–315. <https://doi.org/10.1038/nature10310>, 2011.
- 859 60. Martrat, B., Grimalt, J. O., Shackleton, N. J., de Abreu, L., Hutterli, M.A., and Stocker, T. F.: Four
860 climate cycles of recurring deep and surface water destabilizations on the Iberian Margin, *Science*,
861 317, 502–507, doi:10.1126/science.1139994, 2007.
- 862 61. Marzocchi, A. and Jansen, M. F. Global cooling linked to increased glacial carbon storage via
863 changes in Antarctic sea ice. *Nature Geoscience*, 12, 1001–1005, [https://doi.org/10.1038/s41561-](https://doi.org/10.1038/s41561-019-0466-8)
864 019-0466-8, 2019

- 865 62. Masoum, A., Nerger, L., Willeit, M., Ganopolski, A., and Lohmann, G.: Lessons From Transient
866 Simulations of the Last Deglaciation With CLIMBER-X: GLAC1D Versus PaleoMist, *Geophysical*
867 *Research Letters*, 51(16), e2023GL107310. <https://doi.org/10.1029/2023GL107310>, 2024.
- 868 63. McManus, J. F., Francois, R., Gherardi, J.-M., Keigwin, L. D., and Brown-Leger, S.: Collapse and
869 rapid resumption of Atlantic meridional circulation linked to deglacial climate changes, *Nature*, 428,
870 834–837, 10.1038/nature02494, 2004.
- 871 64. Menviel, L., Yu, J., Joos, F., Mouchet, A., Meissner, K. J., and England, M. H.: Poorly ventilated
872 deep ocean at the Last Glacial Maximum inferred from carbon isotopes: A data-model comparison
873 study. *Paleoceanography*, 32(1), 2–17. <https://doi.org/10.1002/2016PA003024>, 2017.
- 874 65. Menviel, L., Timmermann, a., Timm, O. E., and Mouchet, A.: Climate and biogeochemical response
875 to a rapid melting of the West Antarctic Ice sheet during interglacials and implications for future
876 climate. *Paleoceanography*, 25, 1–12. <https://doi.org/10.1029/2009PA001892>, 2010.
- 877 66. Menviel, L., Timmermann, A., Timm, O. E., and Mouchet, A.: Deconstructing the Last Glacial
878 termination: the role of millennial and orbital-scale forcings, *Quaternary Sci. Rev.*, 30, 1155–1172,
879 10.1016/j.quascirev.2011.02.005, 2011.
- 880 67. Menviel, L., England, M. H., Meissner, K. J., Mouchet, A., and Yu, J.: Atlantic-Pacific seesaw and
881 its role in outgassing CO₂ during Heinrich events. *Paleoceanography*, 29(January), 58–70.
882 <https://doi.org/10.1002/2013PA002542>, 2014.
- 883 68. Menviel, L., Spence, P., Yu, J., Chamberlain, M. A., Matear, R. J., Meissner, K. J., and England, M.
884 H.: Southern Hemisphere westerlies as a driver of the early deglacial atmospheric CO₂ rise. *Nature*
885 *Communications*, 9(1), 1–12. <https://doi.org/10.1038/s41467-018-04876-4>, 2018
- 886 69. Moros, M., De Deckker, P., Perner, K., Ninnemann, U. S., Wacker, L., Telford, R., Jansen, E., Blanz,
887 T. and Schneider, R.: Hydrographic shifts south of Australia over the last deglaciation and possible
888 interhemispheric linkages. *Quaternary Research (United States)*, 102, 130–141.
889 <https://doi.org/10.1017/qua.2021.12>, 2021
- 890 70. Moy, A. D., Palmer, M. R., Howard, W. R., Bijma, J., Cooper, M. J., Calvo, E., Pelejero, C., Gagan,
891 M. K. and Chalk, T. B.: Varied contribution of the Southern Ocean to deglacial atmospheric CO₂
892 rise. *Nature Geoscience*, 12(12), 1006–1011. <https://doi.org/10.1038/s41561-019-0473-9>, 2019

- 893 71. Ng, H. C., Robinson, L. F., McManus, J. F., Mohamed, K. J., Jacobel, A. W., Ivanovic, R. F.,
894 Gregoire, L. J. and Chen, T.: Coherent deglacial changes in western Atlantic Ocean circulation.
895 Nature Communications, 9(1), 1–10. <https://doi.org/10.1038/s41467-018-05312-3>, 2018
- 896 72. Obase, T., and Abe- Ouchi, A.: Abrupt Bølling-Allerød warming simulated under gradual forcing of
897 the last deglaciation, Geophysical Research Letters, 46, <https://doi.org/10.1029/2019GL084675>,
898 2019.
- 899 73. Obase, T., A. Abe-Ouchi, F. Saito: Abrupt climate changes in the last two deglaciations simulated
900 with different Northern ice sheet discharge and insolation, Scientific Reports, 11, doi:
901 10.1038/s41598-021-01651-2, 2021
- 902 74. Parrenin, F., Masson-Delmotte, V., Köhler, P., Raynaud, D., Paillard, D., Schwander, J., Barbante,
903 C., Landais, A., Wegner, A., Jouzel, J.: Atmospheric carbon dioxide, methane, deuterium, and
904 calculated Antarctic temperature of EPICA Dome C ice core. PANGAEA,
905 doi:10.1594/PANGAEA.810199, 2013
- 906 75. Pedro, J. B., Martin, T., Steig, E. J., Jochum, M., Park, W., & Rasmussen, S. O.: Southern Ocean
907 deep convection as a driver of Antarctic warming events. Geophysical Research Letters, 43(5), 2192–
908 2199. <https://doi.org/10.1002/2016GL067861>, 2016
- 909 76. Pedro, J. B., Jochum, M., Buizert, C., He, F., Barker, S., & Rasmussen, S. O.: Beyond the bipolar
910 seesaw: Toward a process understanding of interhemispheric coupling. Quaternary Science Reviews,
911 192, 27–46. <https://doi.org/10.1016/j.quascirev.2018.05.005>, 2018
- 912 77. Peltier, W. R., Argus, D. F., and Drummond, R.: Space geodesy constrains ice age terminal
913 deglaciation: The global ICE-6G_C (VM5a) model, J. Geophys. Res.-Sol. Ea., 120, 450–487,
914 10.1002/2014JB011176, 2015.
- 915 78. Petit, J. R., Jouzel, J., Raynaud, D., Barkov, N. I., Barnola, J.-M., Basile, I., Bender, M., Chappellaz,
916 J., Davis, M., Delaygue, G., Delmotte, M., Kotlyakov, V. M., Legrand, M., Lipenkov, V. Y., Lorius,
917 C., PÉpin, L., Ritz, C., Saltzman, E., and Stievenard, M.: Climate and atmospheric history of the past
918 420 000 years from the Vostok ice core, Antarctica, Nature, 399, 429–436, 10.1038/20859, 1999.

- 919 79. Pöppelmeier, F., Jeltsch-Thömmes, A., Lippold, J. et al. Multi-proxy constraints on Atlantic
920 circulation dynamics since the last ice age. *Nat. Geosci.* 16, 349–356 (2023).
921 <https://doi.org/10.1038/s41561-023-01140-3>
- 922 80. Prange, M., Jonkers, L., Merkel, U., Schulz, M. and Bakker, P: A multicentennial mode of North
923 Atlantic climate variability throughout the Last Glacial Maximum, *Science*, 9, 44,
924 <https://www.science.org/doi/10.1126/sciadv.adh1106>, 2023.
- 925 81. Rae, J. W. B., Burke, A., Robinson, L. F., Adkins, J. F., Chen, T., Cole, C., Greenop, R., Li, T.,
926 Littley, E. F. M., Nita, D. C., Stewart, J. A. and Taylor, B. J.: CO₂ storage and release in the deep
927 Southern Ocean on millennial to centennial timescales, *Nature*, 562, 569–573,
928 <https://doi.org/10.1038/s41586-018-0614-0>, 2018
- 929 82. Renssen, H., Mairesse, A., Goosse, H., Mathiot, P., Heiri, O., Roche, D. M., Nisancioglu, K. H. and
930 Valdes, P. J.: Multiple causes of the Younger Dryas cold period. *Nature Geoscience*, 8(12), 946–949.
931 <https://doi.org/10.1038/ngeo2557>, 2015
- 932 83. Roberts, N. L., Piotrowski, A. M., McManus, J. F., and Keigwin, L. D.: Synchronous Deglacial
933 Overturning and Water Mass Source Changes, *Science*, 327, 75–78, 10.1126/science.1178068, 2010.
- 934 84. Roche, D. M., Renssen, H., Paillard, D., & Levavasseur, G.: Deciphering the spatio-temporal
935 complexity of climate change of the last deglaciation: A model analysis. *Climate of the Past*, 7(2),
936 591–602. <https://doi.org/10.5194/cp-7-591-2011>, 2011
- 937 85. Roche, D.M., Wiersma, A.P. & Renssen, H. A systematic study of the impact of freshwater pulses
938 with respect to different geographical locations. *Clim Dyn* 34, 997–1013.
939 <https://doi.org/10.1007/s00382-009-0578-8>, 2010.
- 940 86. Rojas, M., Moreno, P., Kageyama, M., Crucifix, M., Hewitt, C., Abe-Ouchi, A., Ohgaito, R., Brady
941 E. C. and Hope, P.: The Southern Westerlies during the last glacial maximum in PMIP2 simulations.
942 *Climate Dynamics*, 32(4), 525–548. <https://doi.org/10.1007/s00382-008-0421-7>, 2009
- 943 87. Sadatzki, H., Opdyke, B., Menviel, L., Leventer, A., Hope, J. M., Brocks, J. J., Fallon, S., Post, A.
944 L., O’Brien, P. E., Grant, K., & Armand, L.: Early sea ice decline off East Antarctica at the last
945 glacial-interglacial climate transition, *Science Advances*, 9, 41, doi: 10.1126/sciadv.adh9513, 2023.

88. Schloesser, F., Friedrich, T., Timmermann, A., DeConto, R. M., and Pollard, D.: Antarctic iceberg impacts on future Southern Hemisphere climate, *Nat. Clim. Change*, 9, 672–677, <https://doi.org/10.1038/s41558-019-0546-1>, 2019.
89. Seroussi, H., Nowicki, S., Payne, A. J., Goelzer, H., Lipscomb, W. H., Abe-Ouchi, A., Agosta, C., Albrecht, T., Asay-Davis, X., Barthel, A., Calov, R., Cullather, R., Dumas, C., Galton-Fenzi, B. K., Gladstone, R., Golledge, N. R., Gregory, J. M., Greve, R., Hattermann, T., Hoffman, M. J., Humbert, A., Huybrechts, P., Jourdain, N. C., Kleiner, T., Larour, E., Leguy, G. R., Lowry, D. P., Little, C. M., Morlighem, M., Pattyn, F., Pelle, T., Price, S. F., Quiquet, A., Reese, R., Schlegel, N.-J., Shepherd, A., Simon, E., Smith, R. S., Straneo, F., Sun, S., Trusel, L. D., Van Breedam, J., van de Wal, R. S. W., Winkelmann, R., Zhao, C., Zhang, T., and Zwinger, T.: ISMIP6 Antarctica: a multi-model ensemble of the Antarctic ice sheet evolution over the 21st century, *The Cryosphere*, 14, 3033–3070, <https://doi.org/10.5194/tc-14-3033-2020>, 2020.
90. Severinghaus, J. P. and Brook, E. J.: Abrupt Climate Change at the End of the Last Glacial Period Inferred from Trapped Air in Polar Ice, *Science*, 286, 930–934, [10.1126/science.286.5441.930](https://doi.org/10.1126/science.286.5441.930), 1999.
91. Shakun, J. D., Clark, P. U., He, F., Marcott, S. A., Mix, A. C., Liu, Z., Otto-Bliesner, B., Schmittner, A., and Bard, E.: Global warming preceded by increasing carbon dioxide concentrations during the last deglaciation, *Nature*, 484, 49–54, [10.1038/nature10915](https://doi.org/10.1038/nature10915), 2012.
92. Sherriff-Tadano, S., Abe-Ouchi, A., Yoshimori, M., Ohgaito, R., Vadsaria, T., Chan, W.-L., Hotta, H., Kikuchi, M., Kodama, T., Oka, A., Southern Ocean surface temperatures and cloud biases in climate models connected to the representation of glacial deep ocean circulation, *Journal of Climate*. 3849–3866, <https://doi.org/10.1175/JCLI-D-22-0221.1>, 2023
93. Sigman, D. M., Hain, M. P., & Haug, G. H.: The polar ocean and glacial cycles in atmospheric CO₂ concentration. *Nature*, 466(7302), 47–55. <https://doi.org/10.1038/nature09149>, 2010
94. Sikes, E. L., Schiraldi, B., & Williams, A.: Seasonal and Latitudinal Response of New Zealand Sea Surface Temperature to Warming Climate Since the Last Glaciation: Comparing Alkenones to Mg/Ca Foraminiferal Reconstructions. *Paleoceanography and Paleoclimatology*, 34(11), 1816–1832. <https://doi.org/10.1029/2019PA003649>, 2019.

- 973 95. Sime, L. C., Kohfeld, K. E., Le, C., Wolff, E. W., Boer, A. M. De, Graham, R. M., & Bopp, L.:
974 Southern Hemisphere westerly wind changes during the Last Glacial Maximum: model-data
975 comparison. *Quaternary Science Reviews*, 64, 104–120.
976 <https://doi.org/10.1016/j.quascirev.2012.12.008>, 2013.
- 977 96. Skinner, L. C., Fallon, S., Waelbroeck, C., Michel, E., & Barker, S.: Ventilation of the deep Southern
978 Ocean and deglacial CO₂ rise. *Science*, 328(5982), 1147–1151.
979 <https://doi.org/10.1126/science.1183627>, 2010
- 980 97. Snoll, B., Ivanovic, R.F., Valdes, P.J., Maycock, A. C. and Gregoire, L. J.: Effect of orographic
981 gravity wave drag on Northern Hemisphere climate in transient simulations of the last deglaciation.
982 *Clim Dyn* 59, 2067–2079. <https://doi.org/10.1007/s00382-022-06196-2>, 2022.
- 983 98. Snoll, B., Ivanovic, R., Gregoire, L., Sherriff-Tadano, S., Menviel, L., Obase, T., Abe-Ouchi, A.,
984 Bouttes, N., He, C., He, F., Kapsch, M., Mikolajewicz, U., Muglia, J., and Valdes, P.: A multi-model
985 assessment of the early last deglaciation (PMIP4 LDv1): a meltwater perspective, *Clim. Past*, 20,
986 789–815, <https://doi.org/10.5194/cp-20-789-2024>, 2024.
- 987 99. Steffensen, J. P., Andersen, K. K., Bigler, M., Clausen, H. B., Dahl-Jensen, D., Fischer, H., Goto-
988 Azuma, K., Hansson, M., Johnsen, S. J., Jouzel, J., Masson-Delmotte, V., Popp, T., Rasmussen, S.
989 O., Röthlisberger, R., Ruth, U., Stauffer, B., Siggaard-Andersen, M.-L., Sveinbjörnsdóttir, Á. E.,
990 Svensson, A., and White, J. W. C.: High-Resolution Greenland Ice Core Data Show Abrupt Climate
991 Change Happens in Few Years, *Science*, 321, 680–684, [10.1126/science.1157707](https://doi.org/10.1126/science.1157707), 2008.
- 992 100. Stein, K., Timmermann, A., Young Kwon, E., and Friedrich, T.: Timing and magnitude of Southern
993 Ocean sea ice/carbon cycle feedbacks, *P. Natl. Acad. Sci. USA*, 117, 9,
994 <https://doi.org/10.1073/pnas.1908670117>, 2020.
- 995 101. Stocker, T. F., & Johnsen, S. J.: A minimum thermodynamic model for the bipolar seesaw.
996 *Paleoceanography*, 18(4), 1–9. <https://doi.org/10.1029/2003PA000920>, 2003
- 997 102. Stouffer, R. J., Yin, J., Gregory, J. M., Dixon, K. W., & Spelman, M. J.: Investigating the Causes of
998 the Response of the Thermohaline Circulation to Past and. *Journal of Climate*, 19, 1365–1387.
999 <https://doi.org/10.1002/9781119115397.ch25>, 2006

1000 103.Tarasov, L., Dyke, A. S., Neal, R. M., and Peltier, W. R.: A data-calibrated distribution of deglacial
1001 chronologies for the North American ice complex from glaciological modeling, *Earth Planet. Sci.*
1002 *Lett.*, 315–316, 30–40, 10.1016/j.epsl.2011.09.010, 2012

1003 104.Tierney, J. E., Zhu, J., King, J., Malevich, S. B., Hakim, G. J., & Poulsen, C. J.: Glacial cooling and
1004 climate sensitivity revisited. *Nature*, 584(7822), 569–573. [https://doi.org/10.1038/s41586-020-2617-](https://doi.org/10.1038/s41586-020-2617-x)
1005 *x*, 2020

1006 105.Timmermann, A., Timm, O., Stott, L., and Menviel, L.: The roles of CO₂ and orbital forcing in
1007 driving Southern Hemispheric temperature variations during the last 21 000 Yr. *Journal of Climate*,
1008 22(7), 1626–1640. <https://doi.org/10.1175/2008JCLI2161.1>, 2009

1009 106.Toucanne, S., Zaragosi, S., Bourillet, J.-F., Marieu, V., Cremer, M., Kageyama, M., Van Vliet-Lanoë,
1010 B., Eynaud, F., Turon, J.-L., and Gibbard, P.-L.: The first estimation of Fleuve Manche palaeoriver
1011 discharge during the last deglaciation: Evidence for Fennoscandian ice sheet meltwater flow in the
1012 English Channel ca 20–18 ka ago, *Earth Planet. Sc. Lett.*, 290, 459–473, 2010.

1013 107.WAIS Divide Project Members: Onset of deglacial warming in West Antarctica driven by local
1014 orbital forcing. *Nature*, 500(7463), 440–444. <https://doi.org/10.1038/nature12376>, 2013.

1015 108.WAIS Divide project members: Precise interpolar phasing of abrupt climate change during the last
1016 ice age. *Nature*, 520(7549), 661–665. <https://doi.org/10.1038/nature14401>, 2015

1017 109.Weitzel, N., Andres, H., Baudouin, J.-P., Kapsch, M.-L., Mikolajewicz, U., Jonkers, L., Bothe, O.,
1018 Ziegler, E., Kleinen, T., Paul, A., and Rehfeld, K.: Towards spatio-temporal comparison of simulated
1019 and reconstructed sea surface temperatures for the last deglaciation, *Clim. Past*, 20, 865–890,
1020 <https://doi.org/10.5194/cp-20-865-2024>, 2024.

1021 110.Yoshimori, M., Yokohata, T., and Abe-Ouchi, A.: A Comparison of Climate Feedback Strength
1022 between CO₂ Doubling and LGM Experiments, *J. Climate*, 22, 3374–3395,
1023 <https://doi.org/10.1175/2009JCLI2801.1>, 2009.

1024 111.Zhu, J. and Poulsen, C. J.: Last Glacial Maximum (LGM) climate forcing and ocean dynamical
1025 feedback and their implications for estimating climate sensitivity, *Clim. Past*, 17, 253–267,
1026 <https://doi.org/10.5194/cp-17-253-2021>, 2021.

1027

